
Research manuscript

Modelling the agricultural soil landscape of Germany – A data science approach involving spatially allocated functional soil process units

Mareike Ließ ^{1*}

¹ Department of Soil System Science, Helmholtz Centre for Environmental Research – UFZ, Halle (Saale), Germany; mareike.liess@ufz.de

* Correspondence: mareike.liess@ufz.de

Abstract: The national-scale evaluation and modelling of the impact of agricultural management and climate change on soils, crop growth, and the environment require soil information at a spatial resolution addressing individual agricultural fields. This manuscript presents a data science approach which agglomerates the soil parameter space into a limited number of functional soil process units (SPUs) which may be used to run agricultural process models. In fact, two unsupervised classification methods were developed to generate a multivariate 3D data product consisting of SPUs, each being defined by a multivariate parameter distribution along the depth profile from 0 to 100 cm. The two methods account for differences in variable types and distributions and involve genetic algorithm optimization to identify those SPUs with the lowest internal variability and maximum inter-unit difference with regards to both, their soil characteristics and landscape setting. The high potential of the methods was demonstrated by applying them to the agricultural German soil landscape. The resulting data product consists of twenty SPUs. It has a 100 m raster resolution in the 2D mapping space, and its resolution along the depth profile is 1 cm. It includes the soil properties texture, stone content, bulk density, hydromorphic properties, total organic carbon content, and pH.

Keywords: digital soil mapping, soil process units, soil parameter space, machine learning, unsupervised classification.

1 Introduction

Global food security, the protection of our groundwater resources, and our efforts to combat climate change largely depend on the sustainable use of soils. This concerns the strategic planning of an adequate crop rotation, the careful use of fertilizers, and the restricted use of pesticides. To maintain the soils' high productivity, we need to provide crops with sufficient and easily accessible nutrients. However, the soil's storage potential is limited. Surplus fertilizer contaminates valuable water resources when it percolates to the groundwater. It enhances global warming while released as greenhouse gases into the atmosphere. Furthermore, crops also require sufficient plant-available soil water resources in their respective development stages. Irrigation needs to be crop- and soil-specific but may not be the best solution as it restricts water for other uses. In consequence, it requires thoughtful planning of an adapted crop cycle involving drought-tolerant cultivars (1) and respective soil water management by alternative means (2,3).

All decisions and their consequences with regards to soil productivity and environmental impact ultimately depend on the soil characteristics on site. Accordingly, the national-scale evaluation and modelling of the impact of agricultural management and climate change on agricultural soils, yields, and the environment require information on the multivariate 3D soil parameter space at a spatial resolution addressing individual agricultural fields (4,5). This concerns the assessment of the soils' agricultural productivity (6) and the restrictions and required adaptations due to pro-longed drought periods. Crop phenology models (7) and the evaluation and modelling of soil-related drought (8–10), and corresponding irrigation requirements (11) could be improved to a large extent by adequate soil information at a high spatial resolution. The same applies to the evaluation of the soils' storage potential for soil organic carbon (12,13), the

modelling of the complex processes causing the release of greenhouse gases to combat climate change (14), and the modelling of mitigation options to reduce nitrate pollution (15,16).

Running agricultural process models at national scale requires information about the multivariate 3D soil parameter space at a spatial resolution targeting individual agricultural fields. With a spatial resolution of 100 m this already amounts to about 20 million raster cells for the agricultural soils of Germany. Process models require high computing capacities to run repeated simulations considering agricultural management and climate scenarios on this number of raster cells. Unfortunately, this also goes along with an unnecessary high amount of energy consumption counteracting our efforts to combat climate change. Hence, a creative data science approach is required to agglomerate the information contained in the raster cells to a limited number of spatially allocated functional soil process units (SPUs). This enables us to reduce the required resources without having to accept a lower spatial resolution.

One might argue why not rather use the spatial map units (SMUs) contained in conventional soil maps as SPUs? For Germany there are mainly three reasons why the contained soil information is inappropriate: **[1]** The best conventional soil map available at national scale for Germany is the BÜK at a map scale of 1:250.000 (17). Its SMUs each define a paragenesis of soil systematic units (SUs) with highly differing characteristics. The spatial allocation of these SUs within the SMUs is unknown. Hence, the contained information is not site-specific when it comes to addressing individual agricultural fields. **[2]** Important soil properties guiding soil functionality are only distinguished at a low hierarchical level of the German soil classification system KA (18). Rather similar soils concerning their properties and functionality are assigned to different upper-level SUs. This particularly applies to the particle size distribution which is one of the most important properties guiding soil functionality. **[3]** Last but not least, the BÜK is uncertain. All soil maps are. However, on the one hand, the BÜK's uncertainty is unknown. On the other hand, its uncertainty likely differs between the federal states as the map was developed by slightly differing approaches at the regional soil survey institutions and then later joined and harmonized concerning inconsistencies at the regional boundaries.

The development of creative data science approaches to provide spatially continuous soil information relates to the research field pedometrics. Pedometrics is an interdisciplinary science that integrates soil science with geoinformatics and data science. Pedometric modelling approaches are used to investigate the spatial-temporal variation of the soil landscape and derive spatially continuous soil information from soil profile data. They rely on the concept model of pedogenesis with soils and their vertical profile differentiation and characteristics being the product of the site-specific interaction of the soil-forming factors through long periods of time (19). The conceptual approach was extended by McBratney et al. (20) to include geographic location and proxies for soil itself. The resulting SCORPAN factors include S (proxies to soil), C (climate), O (organisms including land use, agricultural management etc.), R (relief), P (parent material), A (age), and N (geographic location). They are each approximated by spatially continuous gridded data proxies from either remote sensing, by conducting a digital terrain analysis, and/or by including expert knowledge. Padarian et al., Arrouays et al., and Chen et al. (21–23) provide recent reviews. Many studies refer to pedometric modelling for landscape-scale predictions by the terms 'digital soil mapping' or 'predictive soil mapping'. I prefer the term pedometric modelling since digital soil maps are also created by other approaches and any map is two-dimensional, and, therefore, does not necessarily include 3D data products.

Current approaches in pedometric modelling to generate nationwide soil information predominantly address the prediction of individual soil properties. Žižala et al. and Gebauer et al. (24,25) provide recent 2D applications, Malone and Searle and Reddy et al. (26,27) 2.5D applications, and Padarian et al. and Ma et al. (28,29) 3D applications. However, the separate modelling of individual soil properties and their respective joint consideration as input to agricultural process models may result in constructed soil profile information which does not occur in reality and which may be unrealistic according to the underlying pedogenetic processes and dependencies between the properties. Ließ et al. (4) provide a promising alternative for the joint modelling of multiple soil properties in 3D. The resulting data product represents the multivariate 3D soil parameter space of the nationwide agricultural landscape of Germany in terms of spatially allocated SPUs, each being described by a multivariate parameter distribution along the depth profile from 0 to 100 cm. It includes depth- and property-wise uncertainty estimates.

Here, a data science approach shall be developed that serves to generate such multivariate 3D data products consisting of spatially allocated functional SPUs. In contrast to Ließ et al. (4), it involves the development of unsupervised classification methods that account for differences in variable types and distributions and involve optimization to identify those SPUs with the lowest internal variability and maximum inter-unit difference with regards to both, their soil

characteristics and landscape setting. The approach shall be evaluated by applying it to the German agricultural soil landscape to improve the previously mentioned data product.

2 Material and methods

2.1 Data

2.1.1 Soil profile data – Consistency check and gap filling

The soil profile data from the agricultural soil inventory Germany (30) was used for this study. The data was collected by systematic sampling along an 8×8 km grid at 3,104 sites. Each soil profile has an identifier and geographic coordinates. The data comprises field data (data_F) in terms of a soil profile description according to the German soil survey system KA5 (18), and laboratory data (data_L). From data_F , the horizon-wise texture class, stone content, and the horizon symbol of all profiles were considered. From data_L , the particle-size distribution (3 particle size separates), the bulk density, stone content, total organic carbon content (TOC), and the pH value of all profiles were considered. In the following, I describe the consistency check, subsequent data modification, and gap filling procedure which were applied prior to any further analysis.

The sampling protocol for the Agricultural Soil Inventory states that samples for subsequent laboratory analysis ought to be taken for the depth increments 0–10, 10–30, 30–50, 50–70, and 70–100 cm while taking into account horizon boundaries, i.e. including multiple samples per depth increment for each corresponding soil horizon present with five or more centimetres (31). However, as could be expected for such a large soil survey campaign involving multiple teams, the dataset contains some inconsistencies. To combine data_F and data_L , the two datasets were checked for mismatches in absolute profile depth, and horizon sequence notation (term used for data_F and data_L), as well as non-compliant data entries, duplicates or gaps in the horizon sequence notation. After correcting non-compliant data entries, the next correction step concerned the mismatches in profile depth and horizon sequence notation. For their correction, I tested whether mismatches concerning depth and horizon sequence notation corresponded to additional layers (or horizons) and whether the difference was minor to 5 cm, i.e. mismatches in line with the sampling protocol. After adjusting the layer boundaries accordingly, all other mismatches were corrected stepwise by favouring the profile depth of data_F over data_L in case the difference was not caused by additional layers (or horizons), and by splitting layers of data_L if they included one or more horizon boundary which differed from the upper or lower layer boundary by five or more centimetres. This procedure resulted in matching horizon sequence notation and profile depth between data_F and data_L and the two datasets were combined using the profile identifier. From now on, these joint depth divisions will be referred to as horizons.

The modifications in the horizon sequence notation in data_L and data_F resulted in data gaps concerning all laboratory or field data of a certain depth interval. And using interpolation methods to fill these gaps may not be the best option due to the geological stratification, i.e. discontinuities in the soil profiles. In addition, the data gaps relating to the uppermost and last soil horizon cannot be filled in this way. Therefore, the following procedures were applied: The resulting texture data gaps in data_L were filled by additionally considering texture data from data_F . The mean value of the sand, silt and clay content (data_L) from other horizons with matching texture classes (data_F) was used. This happened stepwise. If the prerequisites were met, only data from the same profile was used. Otherwise the complete dataset's respective class-wise mean values were assigned. Finally, the remaining texture classes were filled by the KA5 texture class' mean sand, silt, and clay content. The latter corresponds to layers with uncommon soil texture classes and hence too few data entries (less than five). For data gaps in the TOC of organic soil horizons, a similar approach was followed considering horizon symbols and organic texture classes. For TOC in the mineral soil horizons, as well as the

pH, bulk density and stone content of all horizons, random forest (RF) models were trained. Model training, tuning, and evaluation were conducted with nested stratified cross-validation (CV) as explained in Section 2.4.2. As predictors, the same property's values from upper and lower horizons as well as related soil properties of over- and underlying horizons were used. Related properties of the same horizon could not be used unless for those where data_F was used to fill gaps in data_L.

After gap filling, some additional variables were created. For the stone content, the data from data_F and data_L were combined by assigning the maximum of the two values. This was done since on the one hand, data_L underestimates the stone content with regards to large rock fragments beyond the size of the steel cores used for sampling. On the other hand, the visual method applied to estimate the stone content in data_F may neglect smaller rock fragments. Concerning hydromorphic features, one variable was created for each, the presence (value = 1) or absence (value = 0) of stagnic and gleyig properties, and named symbol_S and symbol_G. The information was derived from the horizon symbology of data_F. An additional variable 'mob' was included in the dataset assigning each horizon to either 'mineral', 'organic', or 'bedrock' by considering the TOC, horizon symbology, and the availability of texture data. Each profile was then subdivided into 1 cm slices up to a depth of 100 cm.

2.1.2 Data cube of covariates

The covariates included to train and apply the machine learning models for nationwide spatial prediction were grouped according to the SCORPAN factor they represent. Table 1 gives an overview. Ließ et al. (4) provide a description of the German landscape setting.

Concerning SCORPAN C, seasonal averages of air temperature and drought, and the sum of precipitation of the winter (Dec., Jan., and Feb.) and the summer (Jun., Jul., and Aug.) months were derived from the German Weather Service.

To approximate SCORPAN O, the following covariates were included: Sentinel-2 data composites of the second yearly quartile of 2018 and 2021 of the bands B01, B02, B03, B04, B05, B06, B07, B08, B8a, B11, and B12 as well as the vegetation indices EVI, MSI, NDMI, NDVI, NDWI, and PSRI (please see Table 1 for the details). The composites were compiled using the Sentinel-Hub on behalf of the surface reflectance values, from the Level 2A product. The composites were downloaded as multiple tiles in 20 m spatial resolution, then mosaicked and resampled to the 100 m INSPIRE — Infrastructure for Spatial Information in Europe — grid topology (32) before calculating the vegetation indices. Additionally, remote sensing products on dry matter productivity (DMP) and the Vegetation Productivity Index (VPI) of the time slot June 11th-20th of the years 2016 and 2018 were derived from the Copernicus Global Land Service. All SCORPAN O covariates seek to capture the main annual phase of agricultural productivity.

SCORPAN R was represented by the Geomorphographic map of Germany and terrain parameters derived by digital terrain analysis with the SAGA — System for Automated Geoscientific Analyses (33) from the EU-DEM digital elevation model.

The map of the "Groups of soil parent material" was included to approximate SCORPAN P. Lithology and stratigraphy according to the hydrogeological map of Germany were additionally incorporated.

Table 1: Covariates

Soil form- ing factor	Abbreviation	Description	Data source
Climate	PRESU	Average seasonal precipitation (summer) [raster, 1000 m]	(65)
	PREWI	Average seasonal precipitation (winter) [raster, 1000 m]	
	TEMSU	Average seasonal temperature (summer) [raster, 1000 m]	(66)
	TEMWI	Average seasonal temperature (winter) [raster, 1000 m]	
	DINSU	Average seasonal drought index (summer) [raster, 1000 m]	(67)
	DINWI	Average seasonal drought index (winter) [raster, 1000 m]	
Organisms/ Soil	B0118, 0218,...B0818, B8A18, B1118, B1218	Sentinel-2 spectral bands B1, B2,...B8, B8A, B11, and B12 composites of the 2 nd yearly quartile of the year 2018	
	B0121, 0221,...B0821, B8A21, B1121, B1221	Sentinel-2 spectral bands B1, B2,...B8, B8A, B11, and B12 composites of the 2 nd yearly quartile of the year 2021	
	EVI18, EVI21	Enhanced vegetation index, calculated from Sentinel 2 band composites of 2 nd quartile 2018 & 2021 (S2-Q2-18/21), $EVI = G \cdot (B8A - B04) / (B8A + C1 \cdot B04 - C2 \cdot B02 + L)$, with $G = 2.5$, $C1 = 6$, $C2 = 7.5$ and $L = 1$	
	MSI18, MSI21	Moisture index: S2-Q2-18/21, $MSI = B11/B08$	
	NDM18,	Normalized difference moisture index: S2-Q2-18/21, $NDMI = (B08 - B11) / (B08 + B11)$	
	NDV18,	Normalized difference vegetation index: S2-Q2-18/21, $NDVI = (B08 - B04) / (B08 + B04)$	
	NDW18,	Normalized difference water index: S2-Q2-18/21, $NDWI = (B03 - B08) / (B03 + B08)$	
	PSR18,	Plant senescence reflectance index: S2-Q2-18/21, $PSRI = (B04 - B02) / B06$	
	DMP16	Dry matter productivity, June 2016 [raster, 300 m]	(68)
	DMP18	Dry matter productivity, June 2018 [raster, 300]	
	VPI16	Vegetation Productivity Index, June 2016 [raster, 300 m]	(69)
	VPI18	Vegetation Productivity Index, June 2018 [raster, 300 m]	

Table 1 (continued): Covariates

Soil form- ing factor	Abbreviation	Description	Data source
Topogra- phy	GMK00	Geomorphographic map of Germany [raster, 250 m resolution, map scale 1:1,000,000]	(70)
	DEM00	Digital elevation model [raster, 25 m resolution]	(71)
	SLO01, SLO05, SLO10	Slope: calculated from DEM (cfD) with a search radius of 1, 5, 10 cells, using SAGA module Morphometric features	(71)
	NOR01, NOR05, NOR10	Northness: derived from aspect cfD with a search radius of 1, 5, 10 cells, using SAGA module Morphometric features	
	EAS01, EAS05, EAS10	Eastness: derived from aspect cfD with a search radius of 1, 5, 10 cells, using SAGA module Morphometric features	
	TST01, TST05, TST10	Terrain surface texture: cfD with a search radius of 1, 5, 10 cells, using SAGA module Terrain Surface Texture	
	TSR01, TSR05, TSR10	Terrain surface ruggedness: cfD with a search radius of 1, 5, 10 cells, using SAGA module Terrain Ruggedness Index	
	CON01, CON05, CON10	Convergence Index: cfD with a search radius of 1, 5, 10 cells, using SAGA module Convergence Index (Search Ra-	
	SLH00	Slope Height: cfD using SAGA module Relative Heights and Slope Positions	
	VAD00	Valley depth: cfD using SAGA module Relative Heights and Slope Positions	
	NOH00	Normalised Height: cfD using SAGA module Relative Heights and Slope Positions	
	WIN00	Wind Exposure: cfD using SAGA module Wind Effect	
	NOP00	Negative openness: cfD using SAGA module Topographic Openness	
	POP00	Positive openness: cfD using SAGA module Topographic Openness	
	VOF0S	Vertical overland flow distance to all river segments: cfD using SAGA module Terrain analysis / Channels	
	VOF0M	Vertical overland flow distance to major rivers: cfD using SAGA module Terrain analysis / Channels	
	HOF0S	Horizontal overland flow distance to all river segments: cfD using SAGA module Terrain analysis / Channels	
	HOF0M	Horizontal overland flow distance to major rivers: cfD using SAGA module Terrain analysis / Channels	
	SWI00	SAGA wetness index: cfD using SAGA module SAGA Wetness Index	
Parent ma- terial	LIT00	Lithology, Hydrogeological map of Germany, HÜK [polygon shapefile, map scale 1:250,000]	(60)
	STR00	Stratigraphy, Hydrogeological map of Germany, HÜK [polygon shapefile, map scale 1:250,000]	(59)
	BAG00	Groups of soil parent material in Germany [polygon shapefile, map scale 1:5,000,000]	
Soil	BGL00	Soil scapes in Germany [map scale 1:5,000,000]	(58)
	DMP86	Dry matter productivity, DMP18–DMP16 [raster, 300 m]	
	VPI86	Vegetation Productivity Index, VPI18–VPI16 [raster, 300 m]	
Geographic location	LAT00	INSPIRE Latitude	(32)
	LON00	INSPIRE Longitude	

Proxies to soil itself (SCORPAN S) can generally be included in the form of conventional soil polygon maps, and remote sensing products relating to soil properties. Regarding the former, the map of the German soil scapes was included. Concerning the latter, differences in DMP and VPI between the dry year 2018 and the rather wet year 2016 were included. They relate to crop phenology affected by drought and, therefore, to the root zone plant-available soil water capacity. All covariates were resampled to the INSPIRE grid topology at 100 m resolution (32). This resolution was chosen as a compromise between the ambition to provide soil information for individual agricultural fields and a restrictive use of computing capacities. The nearest-neighbour method was used for categorical predictors, and B-spline interpolation was applied for numeric predictors. INSPIRE latitude and longitude were additionally included to represent the geographic location (SCORPAN N), and particularly to represent spatial patterns not captured by the other data proxies. The national border and coastline of Germany were derived from the digital land model at map scale of 1:250,000 (version 2.0) provided by the Federal Agency for Cartography and Geodesy (© GeoBasis-DE / BKG, 2020).

2.2 Differentiation of functional SPUs

The nationwide data product is composed of a limited number of spatially allocated functional SPUs each being defined by a multivariate parameter distribution along the depth profile. Each SPU's internal variability is described by a probability density distribution of all considered soil properties in all 1 cm depth slices. Two data science approaches were developed to derive SPUs with the lowest possible internal variability and maximum inter-unit difference with regards to both, their soil characteristics and landscape setting. They are unsupervised classification methods, rely on the Partitioning-Around-Medoids (PAM) algorithm (34) and involve optimization. Furthermore, they address the major concern that the joint consideration of mixed variable types (categorical and numerical) and variables of different distribution and scale have on the clustering result. Ahmad and Khan (35) and Van Mechelen et al. (36) provide an overview. In this particular case, there are variables with 1-0 coding for presence-absence type variables (symbol_S, symbol_G), variables with many zero values (stone content), variables with a threefold distribution (texture represented by sand, silt, and clay content), and variables with a bimodal distribution (TOC, bulk density) due to the inclusion of profiles which are all-mineral and profiles composed of mineral and organic horizons. PAM clustering after a mere data transformation did not yield satisfying results.

The two approaches will be described in the following sections. However, two aspects concern the methodology of both approaches:

1. The gap-filled, sliced (1 cm slices) profile data was used to calculate individual property distance matrices. First, the data were normalized to a range between 0 and 1, considering all slices in all profiles except for texture. For texture, the composites' relation of sand, silt, and clay content were kept summing up to 1. Then the mean of the slice-wise Euclidian profile distance was calculated for each variable and stored in separate distance matrices. Non-defined distances in case of differences in soil material causing missing data, e.g. missing texture data for organic horizons or slices assigned to bedrock, were assigned the maximum distance occurring between any two profile slices for the respective soil property. These property-wise distance matrices were then again normalized resulting in a minimum distance of 0 and a maximum distance of 1. From now on they will be referred to as normalized single-property distance matrices (*nSPdist*).
2. The respective input parameter vectors of the involved optimization process to extract the SPUs are evaluated on behalf of a complex objective function. It seeks to identify those SPUs with the lowest

possible internal variability and maximum inter-unit difference with regards to both, their soil characteristics and landscape setting. The former is evaluated by using the Silhouette Index (34). The latter requires the training of machine learning models to capture the soil-landscape relation and evaluate their predictive performance. A simple and fast learner is required to reduce the required computation time. The Random Forest (RF) algorithm (37) was chosen to suit this purpose. It is described in Section 2.3.1.1.

2.2.1 Approach 1 | PAMp, SPU extraction by P weights optimization

Approach 1 seeks to get the optimal SPUs in terms of the lowest property-wise predictive RMSE from pedometric model training by simultaneously optimizing the number of clusters $nclus$ and the weights $Pw_1, Pw_2, Pw_3, \dots, Pw_p$ (p = number of soil properties) applied to the $nSPdist$. The weights give the inter-profile distances with regards to certain soil properties higher or lower importance compared to others. To avoid confusion, the weights will from now on be termed P weights (property weights). Approach 1 will, therefore, be named PAMp. The objective function evaluated for each of the number of n parameter vectors of $z = 8$ components (seven P weights and $nclus$) evaluated in each iteration step of the optimization is shown in Figure 1. It consists of the following parts:

1. $Pw_1, Pw_2, Pw_3, \dots, Pw_p$ in the range $[0.1, 1]$ are assigned to each $nSPdist$, which are then combined by calculating the weighted average ($dist$). The values of the resulting distance matrix are normalized to the range $[0, 1]$.
2. PAM clustering is conducted on the normalized distance matrix ($ndist$) with $nclus = 8, 9, \dots, 100$. The $nclus$ minimum value was selected according to Ließ et al. (4). For each input parameter vector including $Pw_1, Pw_2, Pw_3, \dots, Pw$ and $nclus$, the best cluster solution is selected on behalf of the Silhouette Index.
- 3.1 The resulting clustering solution $Rdata_{in}$, which assigns each soil profile to one cluster, is then combined with the respective l covariates' values x_1, x_2, \dots, x_l of each profile ($Pdata$) to compile the predictor-response dataset ($PRdata$). The data were subdivided into 5 folds for a stratified 5-fold CV (Section 2.4.2). Categorical covariate values with zero data instances in any of the folds were removed.
- 3.2 Each profile's property-wise mean along the depth profile, $Rdata_{in} [y_1, y_2, \dots, y_p]$, was used to compute property-wise means per cluster.
4. An RF model was trained by 5-fold stratified CV using the $PRdata$ [3.1] as input. The function 'rfsrc' of R package 'randomForestSRC' was used with 1000 trees, a node size of five, and the default setting for the mtry parameter, while imputing no data values.
- 5.1 The previously computed property-wise cluster means [3.2] are assigned to each profile on behalf of the test set RF predictions ($Rdata_{pred}$) generating $Rdata_{pred} [y_1, y_2, \dots, y_p]$.
- 5.2 The property-wise RMSE is calculated using $Rdata_{in} [y_1, y_2, \dots, y_p]$ and $Rdata_{pred} [y_1, y_2, \dots, y_p]$. The objective function value corresponds to the negative mean of the property-wise RMSE values. It is maximized in the optimization process.

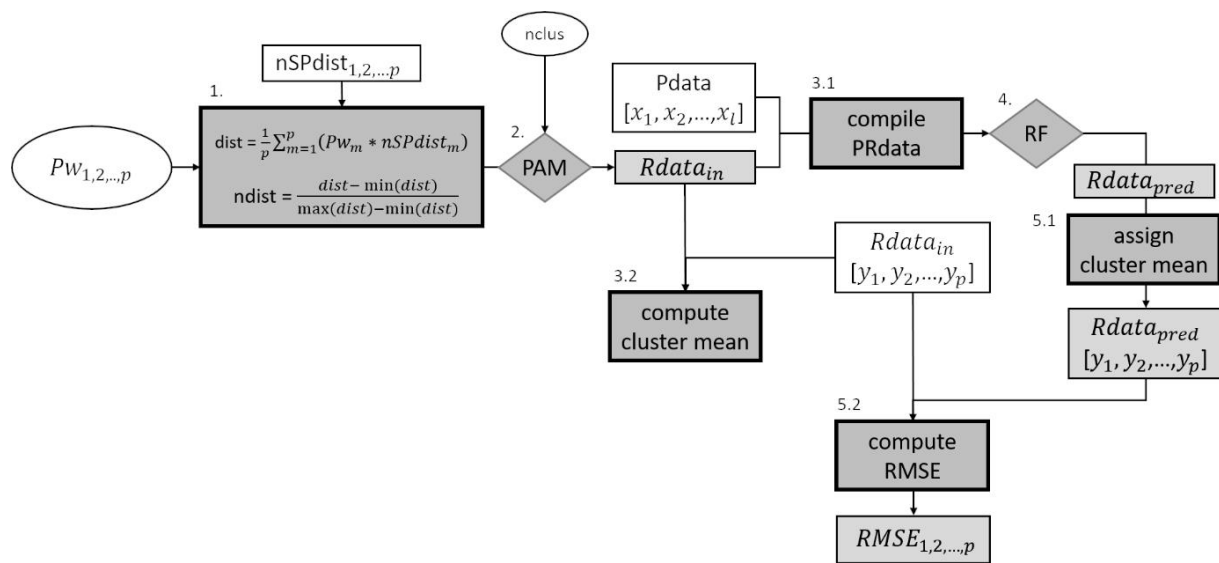


Figure 1: Objective function of the optimization process for SPU differentiation with PAMp. All white boxes are required input data. White ovals reflect parameters which are optimized. Pw = vector of P weights, $dist$ = distance matrix, $ndist$ = normalized distance matrix, $nSPdist$ = normalized single-property distance matrices, $nclus$ = number of clusters, PAM = partitioning around medoids clustering, $Pdata$ = Predictor data, $Rdata$ = Response data, $PRdata$ = predictor-response data, RF = random forest.

2.2.2 Approach 2 | PAMm, SPU extraction by optimized multistep clustering

Approach 2 seeks to get the optimal SPUs in terms of the lowest property-wise predictive RMSE from pedometric model training by applying a multistep clustering with PAM. It will, therefore, be termed PAMm. In this approach, Part 1 and Part 2 of the objective function of PAMp are replaced by the multistep approach (Figure 2). The other subsequent parts remain the same.

The properties considered at each step need to be selected in advance. Optimizing their selection would have increased the complexity of the optimization task and hence required more iterations before convergence. Multistep clustering was conducted in the following way: Step 1 (texture), Step 2 (symbol_S, symbol_G), Step 3 (stone content, bulk density), and Step 4 (TOC, pH). The normalized distance matrices $ndist_1$, $ndist_2$, $ndist_3$, and $ndist_4$ for each step were prepared in advance and then provided as input to the objective function. Each $ndist$ was calculated as the normalized average of the $nSPdist$ of the soil properties considered in the respective step.

In Step 1, PAM is applied to $ndist_1$ testing a number of 2 to ncl_u clusters. The cluster solution with the best Silhouette Index value is chosen unless there are cluster solutions with a sufficiently good Silhouette Index value equal to or above the threshold sil_1 . In that case, the cluster solution with the maximum number of clusters from all cluster solutions with a Silhouette Index value greater than or equal to sil_1 is chosen. In Step 2, PAM is conducted for each cluster resulting from STEP1. This requires subsetting $ndist_2$ according to the profile IDs which were assigned to the respective higher-level Step1 clusters cl_1, cl_2, \dots and normalizing the distance matrix subsets, which were then named $nd_{cl1}, nd_{cl2}, \dots$. The clusters resulting from Step 2 receive a 2nd cluster identifier, e. g. $cl_{1|1}, cl_{1|2}, cl_{2|1}, cl_{2|2}$ indicate that the two clusters from Step 1 were each subdivided into two clusters in Step 2. This procedure is repeated likewise for Step 3 and Step 4. In order not to force unreasonable splitting into a high number of clusters supported by only a low number of profiles, two criteria are tested after each step: [1] The Silhouette Index value of the nd_z cluster solution needs to be greater than or equal to the threshold value sil_{min} and [2] the number of profiles in each resulting cluster from nd_z needs to have a minimum number of profiles p_{min} . If any of the criteria is not fulfilled, then no subdivision is conducted for the respective higher-level cluster in this step, and all profiles receive the identifier 0. p_{min} is also considered to check whether the upper parameter limit of ncl_u needs to be reduced before running PAM on nd_z . PAM is run in parallel

for the respective profile subsets starting from Step 2. A stopping criterion is included to stop in case Step 2 or Step 3 lead to an overall number of clusters $nclus$ of 100 or more. Seven parameters were optimized in PAMm:

- ncl_u : The maximum number of clusters considered in each step.
- $sil_{1,2,3,4}$: One Silhouette Index threshold value per step.
- sil_{min} : The minimum Silhouette Index value tolerated to accept a lower level clustering solution.
- p_{min} : The minimum number of profiles per cluster.

Table 2 displays the respective parameter ranges. The ranges were chosen according to some test runs.

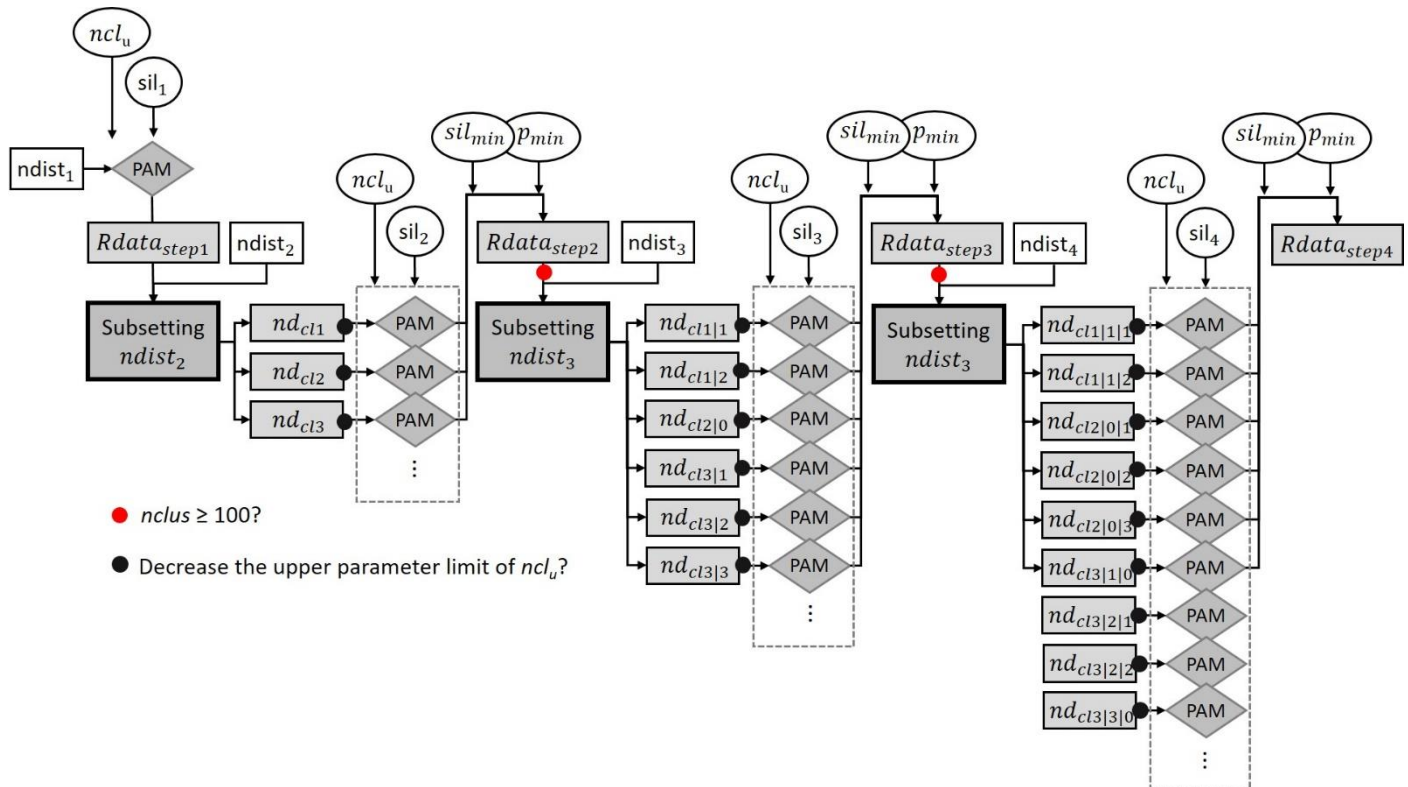


Figure 2: Multistep clustering part of the objective function of the optimization process for SPU differentiation with PAMm. All white boxes are required input data. White ovals reflect parameters which are optimized. $ndist$ = normalized distance matrix, ncl_u = maximum number of clusters to test in each step, sil = threshold of the Silhouette Index, sil_{min} minimum Silhouette Index value, p_{min} minimum number of profiles in each cluster, nd = normalized distance matrix subset, PAM = partitioning around medoids clustering, $Rdata$ = response data, $nclus$ number of clusters.

Table 2: parameter ranges for SPU differentiation by Approach 2

Parameter	Lower limit	Upper limit
ncl_u	3	10
sil_1	0.3	0.4
$sil_{2,3,4}$	0.4	0.8
sil_{min}	0.25	0.4
p_{min}	5	10

2.3 Modelling

The multivariate parameter distributions of the SPUs obtained by PAMp and PAMm are defined by the respective groups of assigned soil profiles. To regionalize the SPUs to the continuous space and to further enhance the extraction of the ready-considered soil-landscape relation, two machine learning models were trained for each of the PAMp and PAMm results using the RF algorithm and the support vector machine (SVM) algorithm. Thus, model training by machine learning was applied for three scopes: [1] for gap filling, [2] for SPU differentiation, and [3] to train the pedometric model fathoming the soil-landscape relation to obtain nationwide and spatially continuous predictions (regionalisation task).

2.3.1 Machine learning algorithms

2.3.1.1 Random forest

The RF algorithm (38) was applied for all three scopes. It is a recursive partitioning method. Depending on the supervised learning task at hand, it either grows multiple regression or classification trees. The results of all trees are averaged. In each tree, the data is subsequently partitioned by the predictor variables into preferably homogeneous subsets regarding the response variable. The mean of each data subset (regression task) or the dominating class (classification task) is then used as the predicted response value. A partition gateway is defined by the predictor and the threshold value in its range, which achieves the most homogeneous partition into two subsets (tree branches). Overall, the stability of the tree ensemble is obtained by training each tree model with a data subset and by using a subset of all predictors. RF is known to achieve reasonable results without tuning, an important characteristic to make it the perfect choice to act as the simple and fast learner for the objective function of the optimization task for Scope [2]. The function 'cforest' of R package 'party', a RF implementation employing conditional inference trees as base learners (39) was used to train the models for gap filling. Model training involved 500 trees (training 1000 trees did not improve model performance in this particular case). The size of the predictor subset (mtry) was tuned via a one-dimensional grid search including one to all predictors. The function 'rfsrc' of R package 'randomForestSRC' (40) was used for the tasks of Scopes [2] and [3]. It provides a fast parallel computing implementation of RF. In both cases, 1000 trees were trained. However, while for Scopes [1] and [3] the mtry parameter was tuned, for Scope [2], the mtry parameter was set to the default to speed up computation time, i.e. use RF as a fast and simple learner.

2.3.1.2 Support vector machine

The SVM algorithm (41) was applied for the regionalisation task (Scope 3) and compared to the RF models. While RF was applied to pay tribute to the fact that the optimization might have favoured a SPUs differentiation whose soil-landscape relation is well captured with RF (learner in the objective function), the SVM algorithm was chosen as a powerful algorithm which led to promising results when capturing the soil-landscape relation to generate the data product of Ließ et al. (4).

SVMs were developed by Cortes and Vapnik (41). In binary classification tasks, they search for the hyperplane that maximizes the margin between the two classes' closest points. The properties of this decision surface ensure the SVM's high generalization ability. Points along the boundary are called support vectors. The data are projected to the higher dimensional space via kernel techniques to allow for separation in case of nonlinearity. The radial basis function kernel was applied for this purpose. It helps to build complex decision boundaries and includes two parameters: C and γ that need to be tuned. The γ parameter can be interpreted as the inverse of the radius of influence of the support vectors. C is the cost or penalty parameter. With a small C, the penalty for misclassified points is low; high values increase the risk of overfitting. Finally, it balances the misclassification of training samples against the simplicity of the hyperplane. R

package “e1071” provides the R interface to the LIBSVM library for SVM (42,43). To allow for multi-class classification, it uses the one-against-one technique by fitting all binary classifiers and finding the correct class by a voting mechanism. The two-dimensional parameter space to search for the optimal parameter combination expands in the following ranges: C [0.01, 100], γ [0.01, 10].

2.3.2 Model training, tuning, and evaluation

For the gap-filling task, the predictor-response dataset consists of horizon-wise data (horizon sequence notation after combining data_l and data_r). For the SPU differentiation and regionalisation tasks, it consists of profile-wise data. All numerical predictors were scaled to the range 0, 1 to avoid misbalance. Categorical data were kept for RF and recoded into dummy variables for SVM. To generate the predictor-response dataset for Scopes [2] and [3], the predictor values were extracted at the soil profile sites, and each soil profile was assigned to a SPU. Concerning SPU differentiation, the latter is done in each iteration step of the objective function as explained in Figure 1. Concerning the regionalization task, the final SPUs obtained respectively by PAMp and PAMm were used.

Model training and evaluation were conducted by a 5-times repeated 5-fold stratified CV (44) to obtain robust models. For the machine learning applications (Scope 1 and Scope 3) involving model tuning via grid search (RF) or optimization (SVM), the CV was nested. The predictor-response dataset was subdivided into five folds of equal size using the response variable for stratification. Of these five folds, then always one fold was kept out as a test set while the other four were combined to form the model training set, leading to five separate test set evaluations (one per data instance). Each of the outer CV's training sets was again subdivided to provide the datasets for parameter tuning in the inner CV cycle. Concerning the categorical predictors, categories not present in all data subsets were removed before model training, tuning, and evaluation. To evaluate model performance the test set predictions were compared to the measured data to calculate the slice-wise RMSE for each of the considered soil properties. The interquartile ranges of the SPUs' multivariate distributions were used for this purpose, i.e. for each considered soil property and depth slice it was tested whether the test set profile measurements fall within the interquartile range of the slice- and property-wise density distributions of the predicted SPU (residual of zero), whether they are smaller than the 25% quantile and how much (positive residual), or whether they are larger than the 75% quantile (negative residual). The five repetitions of the 5-fold CV result in twenty-five models and five RMSE values.

For the RF models to conduct gap-filling, a repeated 5-fold stratified group CV was applied, i.e. all horizons of a profile were assigned to the same fold to avoid overoptimistic test set estimates due to spatial autocorrelation. Concerning the regionalisation task with SVM, the parameter tuning involving optimization was in a first step only conducted on behalf of one out of the twenty-five training sets of the outer CV cycle to check whether this provided satisfying results while the obtained tuning parameter values were applied to all other training sets. Altogether, for the regionalisation with RF and SVM of the SPUs obtained by PAMp and PAMm, four pedometric models were trained. They will be referred to as RF-PAMp, RF-PAMm, SVM-PAMp, and SVM-PAMm.

2.3.3 Variable importance

Concerning gap filling (Scope [1]) with cforest, the package's internal VI measures were used. Concerning the regionalisation task (Scope [3]), a different procedure was followed to allow for the comparison between SVM and RF. For model interpretation, each predictor's importance was obtained by permuting the predictor in the test set before model application. In this way, any predictor-response relationship with regards to that predictor was eliminated. The resulting relative decrease in model performance was then attributed as variable importance (VI) to the respective predictor. Values of five permutations were averaged. The VI values for the dummy variables created from each of the

categorical predictors (SVM) were summed. Due to the five times repeated 5-fold CV approach (outer CV cycle), the VI plots display boxplots of twenty-five VI values for each predictor.

2.4 Genetic algorithm optimization

Genetic algorithm (GA) optimization was applied to differentiate the SPUs (Scope [2]) and to conduct parameter tuning in machine learning (Scope [3]). The GAs' operational structure is inspired by the general principles of biological evolution involving mutation, crossover, selection, and elitism (45). The objective function for Scope [2] was described in Section 2.2 (Figures 1 and 2). The objective Function for SVM parameter tuning (Scope [3]) is done as indicated by Figure 1, Parts 3-5 while replacing Part 4 with SVM. It corresponds to the inner CV cycle (Section 2.3.2). RF (Scope [1] and Scope [3]) does not require optimization for parameter tuning (4).

The parameter space to be searched for the optimal combination of parameter values has to be predefined by providing a minimum and maximum value for each parameter. Then, a random number of n parameter vectors, the parent population, is evaluated by a problem-specific objective function. Weights are assigned to each parameter vector according to its objective function value before starting to modify them by conducting 'selection', 'mutation' and 'crossover' to form a new population of parameter vectors which is again evaluated. This process is iterated until either [1] an initially defined objective function value is achieved by any of the vectors, [2] a maximum number of iterations is reached, or [3] the overall best objective function value does not improve for a certain number of consecutive iterations. GA optimization was run in parallel subdividing the parent population of size 500 into subpopulations and allowing for limited exchange of population individuals (parameter vectors) between the so defined islands. 25 islands (20 parameter vectors per island) were used for the differentiation of the SPUs with PAMp (Scope [2]), and the tuning of the SVM models (Scope [3]). For the differentiation of the SPUs with PAMm (Scope [2]), the number of islands was reduced to 5 resulting in a subpopulation size of 100 per island. The search on the islands was not run in parallel but sequentially due to conflicts that were otherwise caused by the parallelization of the objective function.

3 Results and discussion

3.1 Gap filling

Gap-filling of the soil profile data was needed to calculate the slice-wise distance matrices, and run PAMp and PAMm. The gaps originated from the correction for horizon sequence notation mismatches between data_L and data_F. With an average R^2 between 0.86 and 0.95, all gap-filling models display a very good predictive performance (Figure 3B). The RMSE amounts to a mean value of 0.12 g cm⁻³ for bulk density, 5.9 Vol-% for stones_F, 3.7 Vol-% for stones_L, 5.9 g kg⁻¹ for TOC, and 0.22 for pH (Figures 3A1, 3A2, 3A3, and 3A4). The respective gap-filling of data_L with data_F for the particle size distribution and TOC of organic horizons remains unevaluated. It consists in the consideration of field estimates for those depth increments where laboratory data is missing, a common practice in soil science. The data are of course less precise since the KA5 soil survey instructions identify property classes instead of precise values. Errors in the class assignment were corrected for by the here presented approach.

Data gaps in soil profile data are a common feature. Multiple approaches have been applied including extrapolation to estimate soil properties in deeper soil horizons, gap-filling to provide estimates on behalf of expert knowledge, or assigning values from associated databases (46,47). I am unaware, though, of any other publication documenting the use of multiple soil properties from over- and underlying horizons to train machine learning models to conduct gap filling. However, machine learning algorithms are readily applied to fill spatial data gaps in remote sensing data (48,49) and temporal gaps in time series data (50,51). Another related field is the development of pedotransfer functions to

estimate missing data of soil properties which are laborious to determine from ready available other properties using machine learning. Ghanbarian and Pachepsky (52) provide a review.

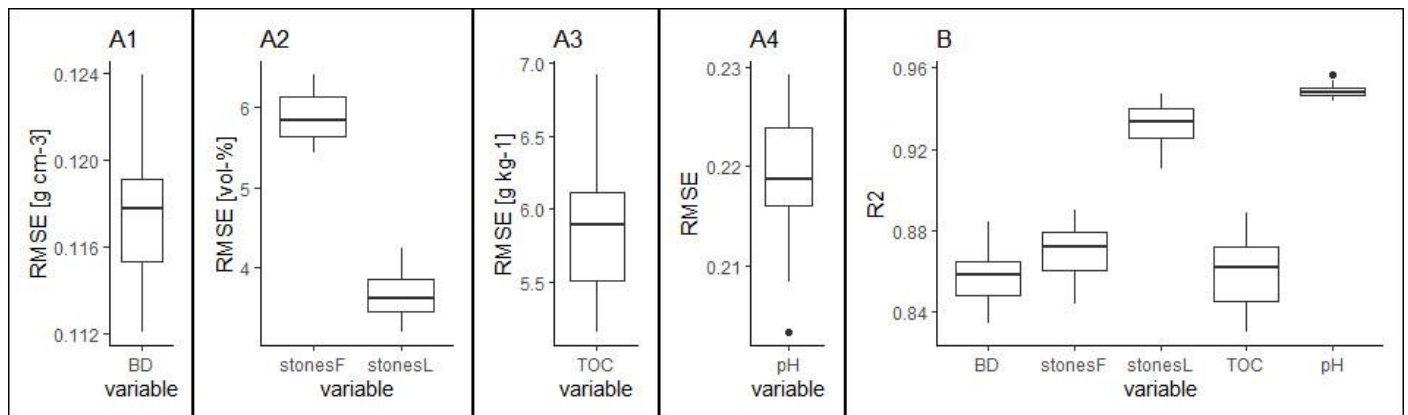


Figure 3: Predictive model performance of the RF models for gap filling. A) RMSE boxplots of twenty-five models, B) R² boxplots of twenty-five models. BD = bulk density, stonesF = stone content from dataF, stonesL = stone content from dataL, and TOC = total organic carbon content.

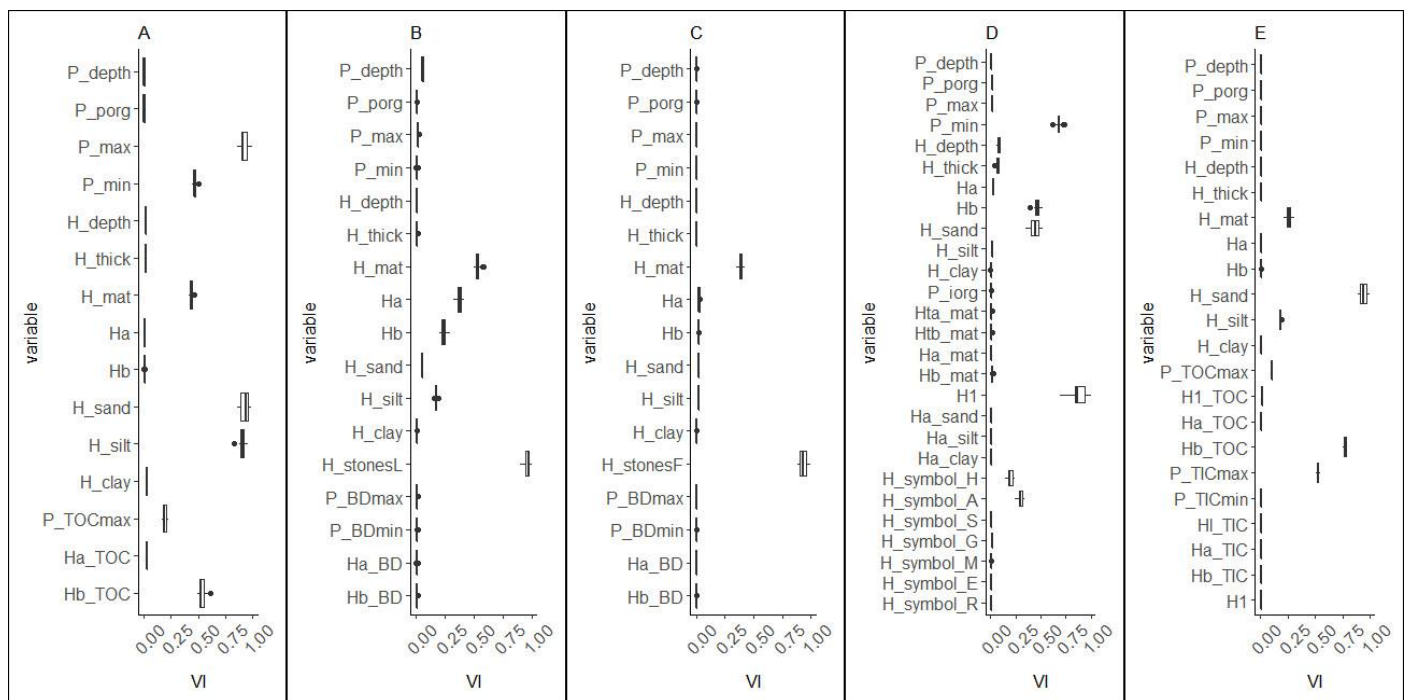


Figure 4: Relative variable importance values (VI) of the RF models for gap filling. A) Bulk density, B) stonesF (stone content from dataF), C) stonesL (stone content from dataL), D) TOC, and E) pH. P_* = value corresponding to the whole profile. H_* = property values of the horizon to be gap-filled. Ha_* property values of the overlying horizon, Hb_* property values of the underlying horizon, H1 = value of the uppermost horizon, Hl = value of the last horizon, porg = percentage of organic horizons, thick = thickness, mat = horizon material (mineral, organic, bedrock).

Figure 4 displays the relative VI values for the respective gap-filling models for bulk density (Figure 4a), stonesL (Figure 4b), stonesF (Figure 4c), TOC (Figure 4d), and pH (Figure 4e). The minimum and maximum profile values, the horizon's material, the horizon's sand and silt content, as well as the underlying horizon's TOC value, were the most important predictors for gap filling bulk density data. The stonesF data was gap-filled detecting the horizon's data: stone content, the horizon's material and the stonesF values of the over- and underlying horizons as main predictors. For stonesL, the

most important predictors were the horizon material and the horizon's data_F stone content. Gap-filling the TOC data indicated the first horizon's TOC value, the underlying horizon's TOC value (below gap), the profile's minimum TOC value, and the horizon's sand content as the most important predictors followed by the horizon's symbol annotation as A-horizon or H-horizon. Although the gap-filling was applied for mineral horizons only, there were still horizons assigned as organic (symbol_H) indicating some questionable assignments during soil profile description in the field. Gap filling pH data indicated the horizon's sand content, the underlying horizon's TOC value, and the profile's maximum total inorganic carbon content as the most important predictors. Overall, several soil properties related to the target property, were detected as important predictors in all cases. Still, for each of the target properties, there are some non-important predictors or predictors with very low VI values. Ultimately, all information which could be of any help for filling gaps with regards to the respective property were included to make sure the result with the lowest predictive uncertainty was obtained.

3.2 Differentiation of functional SPUs

The optimization to differentiate the SPUs resulted in 20 SPUs for PAMP and 47 SPUs for PAMm. Table 3 displays the resulting parameter values for PAMP, and Table 4 reports the values for PAMm. None of the parameter values is close to the upper or lower boundary of the respective parameter range, indicating that they were chosen well.

Table 3: PAMP parameters resulting from optimization to differentiate SPUs.

parameter	<i>P weights</i>							<i>nclus</i>
	texture	stone content	bulk density	symbol_S	symbol_G	TOC	pH	
value	0.24	0.56	0.70	0.51	0.44	0.64	0.86	20

Table 4: PAMm parameters resulting from optimization to differentiate SPUs.

parameter	<i>ncl_u</i>	<i>sil₁</i>	<i>sil₂</i>	<i>sil₃</i>	<i>sil₄</i>	<i>sil_{min}</i>	<i>p_{min}</i>
value	6	0.31	0.74	0.62	0.53	0.34	13

The different *P weights* indicate that the profile distances with regards to the respective soil properties were attributed differing importance by PAMP. The profile distance with regards to texture was given the overall lowest importance, the distance with regards to TOC, bulk density and pH the highest, and the importance of the distance with regards to stone content, symbol_S, and symbol_G ranges somewhere in between. The *P weights* as such are a result of three aspects: [1] the variable types and multivariate distribution in the available soil profile data and considered soil properties, [2] the importance of the profile distances concerning the respective properties for differentiating the clusters, and [3] how well the clusters separate in space on behalf of the available data proxies of the soil-forming factors. Aspect [1] was the reason to develop PAMP, Aspect [2] is due to the fact that for each PAMP input parameter vector the best PAM clustering solution is chosen according to the Silhouette Index, and Aspect [3] concerns the evaluation of the respective cluster solution by the RF predictive performance. As a consequence, the *P weights* cannot be interpreted as a mere soil property importance for clustering.

The optimized parameter values in the second approach, PAMm, do not allow for such a direct interpretation either. The corresponding parameters *sil₁*, *sil₂*, *sil₃*, and *sil₄* merely provide the chance to increase the number of clusters in the respective clustering step of the multistep clustering procedure. Instead of choosing the best cluster solution in each step according to the Silhouette Index, solutions with a sufficiently good Silhouette Index value are accepted. This then

of course also has an impact on the clustering in all subsequent steps. Figure 5 displays the subdivision tree of the step-wise procedure. Step 1 subdivided the profile data into six clusters. The best Silhouette value for this step would have led to a cluster solution with two clusters only. Hence, the sil_1 threshold of 0.31 led to this higher number of clusters obtained on behalf of the profiles' texture data. In Step 2, the subdivision with regards to symbol_S and symbol_G resulted in six clusters for Cluster 1, four for Cluster 3, three for Cluster 4, and six for Cluster 5, while there was no subdivision for Clusters 2 and 6. Six of the overall twenty-one clusters present after Step 2 were not further subdivided in the subsequent steps. Then, after Step 3, the dataset was already so much subdivided that further subdivision resulted in a maximum of two clusters for each of the Step 3 clusters in Step 4. During the optimization process, very different tree structures were tested leading to this overall result. The variables in each step were selected according to their estimated importance for soil functionality. Furthermore, only variables of similar variable type and distribution were considered in each step. Applying the 4 steps in a different sequence would certainly have resulted in a different solution. However, previous test runs had shown this sequence to be the most promising.

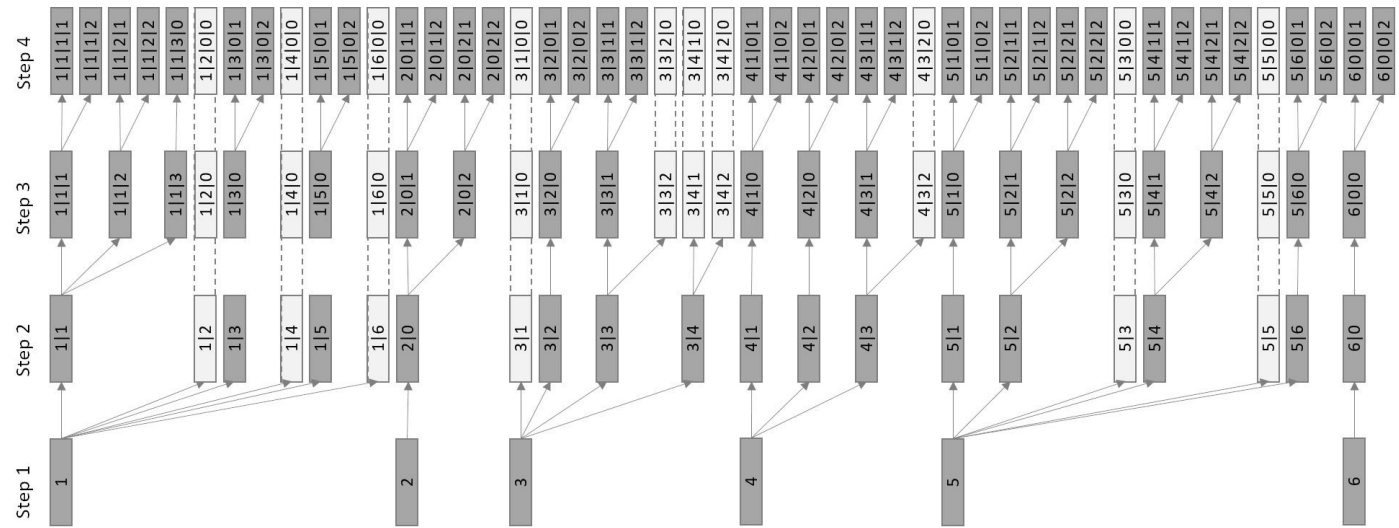


Figure 5: PAMm subdivision tree of the step-wise procedure. The light grey colour indicates that the cluster obtained by the respective step is already a final cluster which will not be further subdivided in the subsequent clustering steps.

Figure 6 shows the multivariate parameter distributions along the depth profile for the 20 SPUs resulting from PAMp. The SPUs were sorted to facilitate their description: One SPU including organic horizons (SPU 1), three leptic-skeletal SPUs (SPU 2 – SPU 4) having a high stone content and depth limitation in the top 100 cm, three skeletal SPUs (SPU 5 – SPU 7), four SPUs differentiated on behalf of their texture and other soil properties (SPU 8 – SPU 11), four stagnic SPUs (SPU 12 – SPU 15), and five gleyic SPUs (SPU 16 – SPU 20). Figures 6A1 – 6A20 display the percentage of soil profiles composed of organic, mineral or bedrock material in the respective depth slice of the SPUs. The corresponding perc_o, perc_m, and perc_b values of the data product published alongside this manuscript replace the symbol_H, symbol_C, and symbol_mC variables of the multivariate distributions of the data product from Ließ et al. (4) in an elegant way. SPU 1 corresponds to agricultural soils that are made up of organic material in one or more horizons along their profile (Figure 6A1). The particle size distribution in its mineral horizonsshow the maximum variation among all SPUs in terms of sand content (Figure 6B1). It lies between 0 – 5% and 96 – 98% taking into account the slice-wise 5 and 95% quantiles of the distribution along the depth profile. Looking at the interquartile range, the variation in sand content in the top 49 cm still ranges between 12 – 25% and 82 – 84%. The overall median TOC, but also the variation in TOC are the highest among all SPUs. Considering the interquartile range, the TOC ranges between 27 – 358 and 331 – 492 kg kg⁻¹

throughout the profile. Regarding the low number of profiles with organic horizons contained in the dataset, this high variation in TOC and soil texture is not surprising. The high variability of soils in SPU 1 cannot be further subdivided by PAMp allowing for a maximum of 100 clusters. And some of the profiles including organic horizons are still included in the other SPUs (compare e.g. Figures 6A12 and 6A14). The same was also reported by Ließ et al. (4). Likewise, a perfect separation into all-mineral and partly-mineral soils in the first step of PAMm had also not resulted successful while the mere assignment to organic or non-organic of the respective slice was considered, or additional soil properties such as TOC (previous test runs) were included. However, a further subdivision of this SPU could likely be achieved by increasing the dataset of these partly-mineral soils. Meanwhile, an alternative could be to conduct a previous subdivision into all-mineral and partly-mineral soils, and then apply PAMp and PAMm to each of the two groups separately.

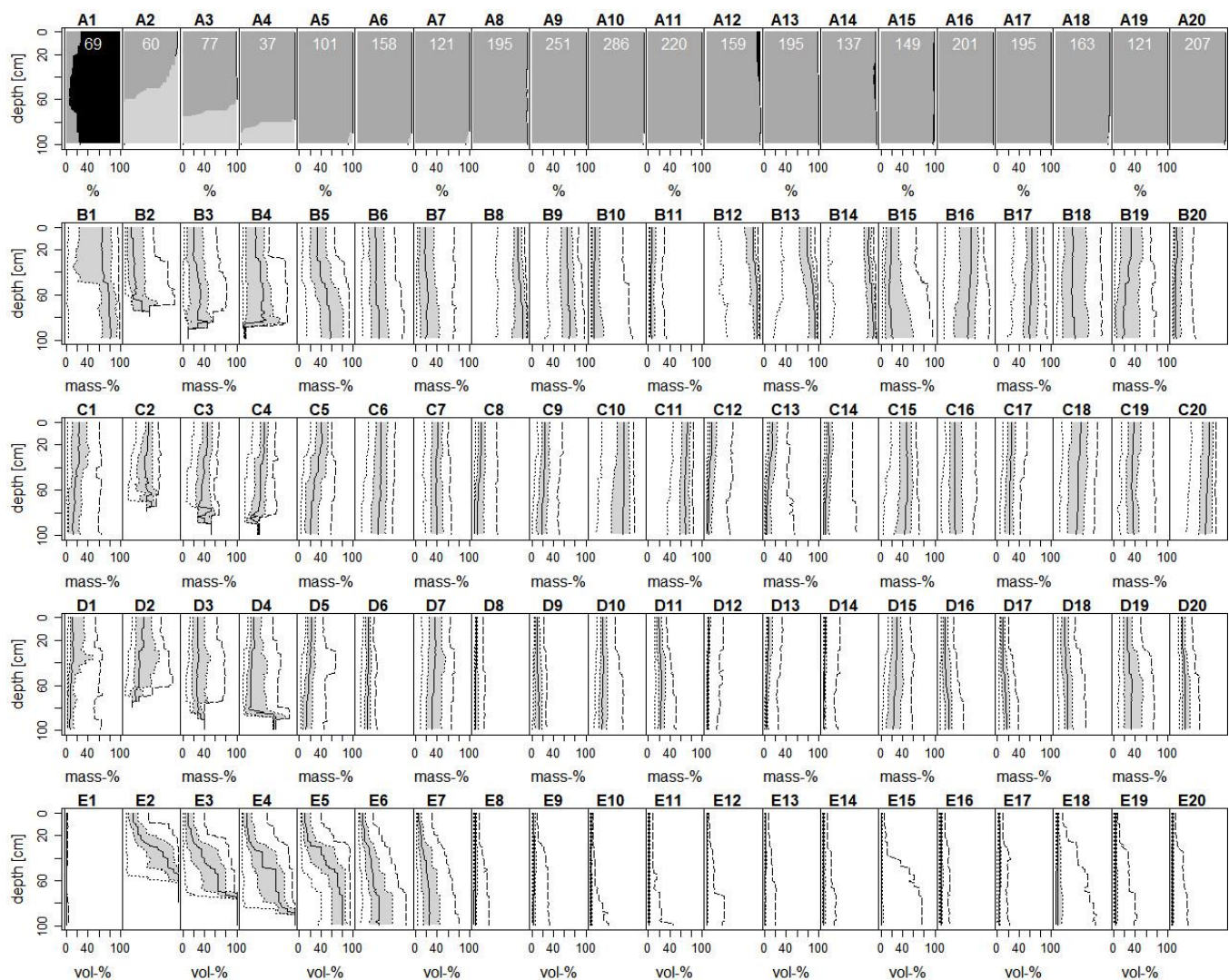


Figure 6, Part 1: Multivariate soil parameter distributions along the depth profile of the SPUs obtained with PAMp. The figure columns reflect the respective SPUs 1 to 20, figure lines refer to the various soil properties. A) indicates the slice-wise contribution of profiles with mineral properties (dark grey), organic properties (black) or bedrock (light-grey). The white numbers indicate the number of profiles supporting the respective SPU. B) sand content, C) silt content, D) clay content, and E) stone content. In Figures (B) to (E), the solid line indicates the median of the distribution, the shaded area between dotted lines reflects the interquartile range, the other dotted line reflects the 5% quantile, and the dashed line reflects the 95% quantile.

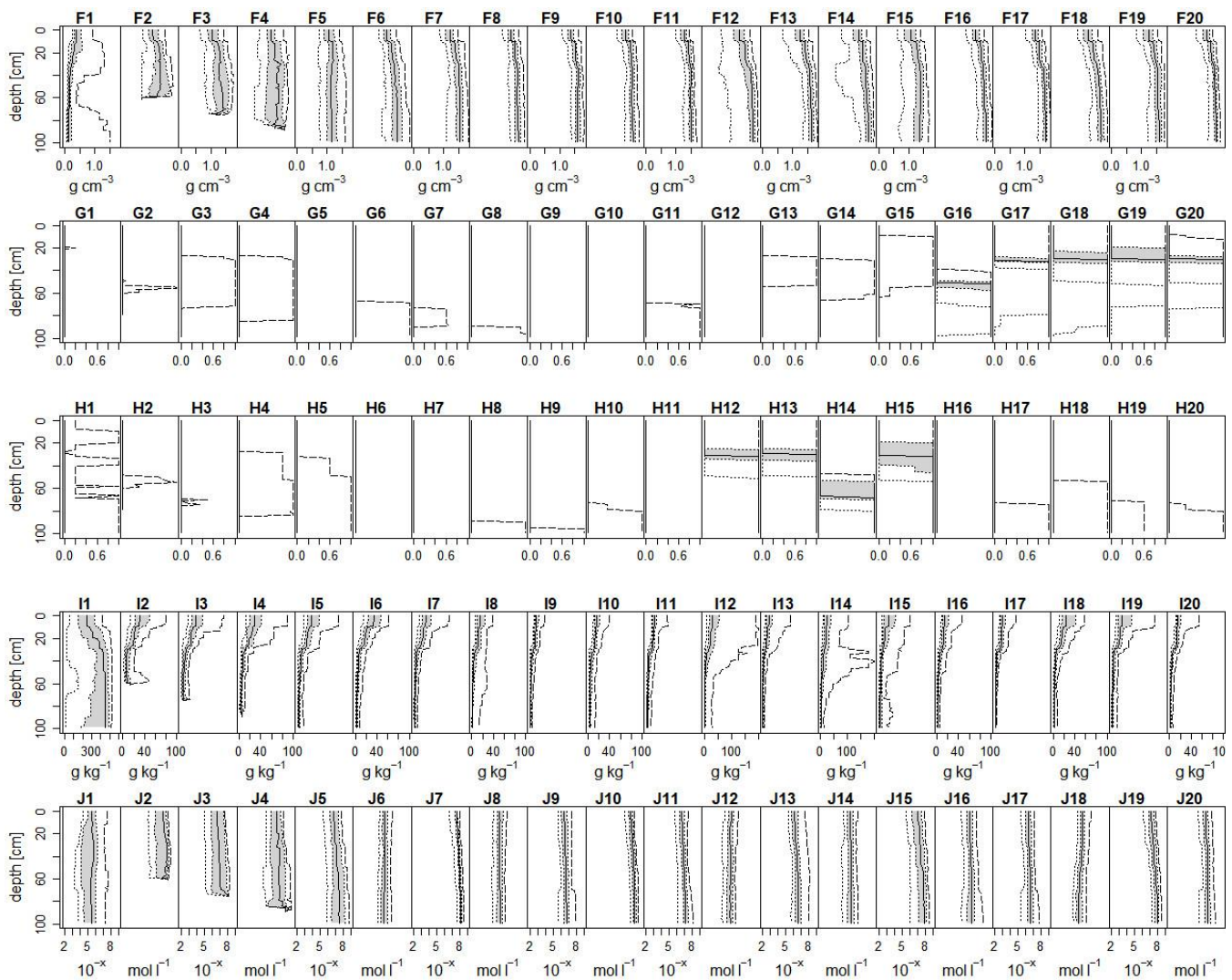


Figure 6, Part 2: Multivariate soil parameter distributions along the depth profile of the SPU solution PAMP. The figure columns reflect the respective SPUs 1 to 20, figure lines refer to the various soil properties. F) bulk density, G) symbol_S, H) symbol_G, I) TOC, and J) pH. The solid line indicates the median of the distribution, the shaded area between dotted lines reflects the interquartile range, the other dotted line reflects the 5% quantile, and the dashed line reflects the 95% quantile. Please be aware that Figures (I) have different X-axis ranges, namely I1) = 0-600, I12) to I15) = 0-200, and all others = 0-100.

The SPUs 2 – 7 have a rather high stone content increasing with depth (Figures 6E2 – 6E7). Of these six SPUs, SPUs 2 – 4 have a depth limitation within the top 100 cm (Figures 6A2 – 6A4). They differ in the strength of this depth limitation, though. SPU 5 displays the same strong increase in stone content with depth comparable to the SPUs 2 – 4, whereas SPU 6 and SPU 7 have a slighter increase. Furthermore, the SPUs 5 – 7 also differ in their particle size distribution: Their sand content is decreasing from SPU 5 to SPU 7 (Figures 6B5 – 6B7).

The SPUs 8 – 11 also have a decreasing sand content (Figures 6B8 – 6B11). I will refer to SPU 8 and SPU 9 as sandy and to SPU 10 and SPU 11 as silty SPUs. Three of these SPUs (SPU 9, SPU 10, and SPU 11) are also the SPUs with the overall highest number of profiles (Figures 6A9, 6A10, and 6A11). Apart from their texture, these four SPUs differ in their pH (Figures 6J8 – 6J11), with SPU 8 having the lowest and SPU 10 the highest pH value. For SPU 8, this corresponds to a pH between 5.2 – 5.6 and 5.9 – 6.0 throughout the profile, for SPU 10 it corresponds to a pH between 7.3 – 7.9 and

7.8 – 8.3 (interquartile range). A similarly high pH value is attributed to SPU 7, SPU 15, and SPU 19, indicating that there is one such SPU in each group: the skeletal SPUs, the texture SPUs, the stagnic SPUs, and the gleyic SPUs.

The SPUs 11 – 20 have hydromorphic properties in some part of their profile. Of these, the SPUs 12 – 15 have a horizon with stagnic properties (Figures 6H12 – 6H15), and the SPUs 16 – 20 indicate ground water influence (Figures 6G16 – 6G20). Still, the presence of the 95% quantile in most of the other SPUs indicates that a few soil profiles with hydromorphic properties have also been assigned to these SPUs. PAM clustering to separate soils with and without stagnic properties and soils with and without gleyic properties merely on the *nSPdist* of symbol_S or symbol_G respectively (test runs) had also not succeeded to provide a perfect separation. Ließ et al. (4) did not achieve this, either. However, it has to be noted that the two SPUs with gleyic and two SPUs with stagnic properties of data product by Ließ et al. (4) were now extended to five and four SPUs respectively. The SPUs 12 – 15 indicate a high TOC consistent with hydromorphic conditions that reduce organic matter decomposition (Figures 6I12 – 6I15). The median TOC in the top 20 cm ranges between 16 and 38 g kg⁻¹ for these SPUs, while it lies between 10 and 16 g kg⁻¹ for the SPUs 8 – 11. The SPUs 2 – 7 and 18 – 19 have a comparatively higher variation in the TOC in their top 10 cm indicating that they include grassland soils. This is reasonable given that SPUs 2 – 7 have high stone contents and are likely to occur in inclined areas and the SPUs 18 – 19 have ground water influence at shallow depth. Furthermore, due to their comparatively lower topsoil TOC values, it is likely that most of the soil profiles assigned to SPU 16, SPU 17 and SPU 20 were drained to be used for crop cultivation or are cultivated with crops that do not mind water logging at a low rooting depth. While the SPUs 12 – 14 have a rather high median sand content and differ due to the depth of their stagnic horizon and their pH value (Figures 6J12 – 6J14), SPU 15 has a low median sand content and corresponding higher silt and clay contents (Figures 6B15, 6C15, and 6D15).

Compared to the data product from Ließ et al. (4) the ranges between the 5 and 95% quantiles and the interquartile ranges of the SPUs' multivariate parameter distributions regarding the particle size distribution, bulk density and stone content were reduced. With regard to the stagnic and gleyic properties, Ließ et al. (4) include prediction probabilities instead of quantiles. These are low in the upper part of the profile, then increase with depth in a transition zone of 30 cm and are high in the lower part of the profile. Considering the interquartile ranges of the multivariate distributions related to symbol_S and symbol_G, these transition zones are smaller for all gleyic SPUs and the stagnic SPUs 12 – 14 but similar for the stagnic SPU 15.

3.3 Pedometric modelling to capture the soil-landscape relation

3.3.1 Model performance

Figure 7 displays the property-wise predictive model performance for the four models RF-PAMp, RF-PAMm, SVM-PAMp, and SVM-PAMm. The performance measure of the approach always depends on two aspects: [1] the statistical dispersion of the multivariate parameter distributions of the SPUs resulting from PAMp or PAMm and [2] the performance of the machine learning algorithm to extract the soil-landscape relation. Consequently, the evaluation of the data product is best achieved in a sense of the predictive RMSE of the individual soil properties.

Regarding soil texture, predictive model performance always detects SVM-PAMp as the best model and RF-PAMm as the least promising, whereas the priority between SVM-PAMm and RF-PAMp favours SVM-PAMm for sand and clay content and RF-PAMp for silt (Figure 7A, 7B, and 7C). SVM-PAMp is also the most promising among the four models concerning its predictive performance in terms of the stone content up to a depth of 60 cm (Figure 7D), the prediction of gleyic properties, and the TOC (Figure 7H). Below 60 cm, RF-PAMp shows the best performance for the stone content (Figure 7D). Additionally, this model has the best performance concerning bulk density (Figure 7E). Predicting pH, SVM-PAMm shows the best performance. However, the RMSE of RF-PAMm and SVM-PAMp are only slightly higher.

Model performance in reference to stagenic properties is hardly distinguishable between the four models until a depth of 30 cm. This similarity continues for SVM-PAMp and RF-PAMp in the subsoil, while the RMSE of RF-PAMm and SVM-PAMm does not increase as much, resulting in RF-PAMm being the overall best for this property. Altogether, this makes SVM-PAMp the best model for three out of seven soil properties and minor differences for a fourth property. This indicates the high power of the SVM algorithm when combined with GA optimization for parameter tuning. In contrast, it was expected that RF might result in the overall better algorithm due to its usage in the objective function for SPU optimization. But the results are ambivalent. RF resulted in the better algorithm for two properties, and SVM for four properties. Overall, this enhances the critical discussion on the common perception that RF is often stated to have the best predictive performance when comparing multiple machine learning algorithms in pedometric modelling applications (53). The comparison is usually not conducted appropriately since RF does not require much tuning and its most important parameters are natural numbers and, therefore, the common grid-search approach is sufficient. In contrast, the training of SVMs requires thorough tuning of real-valued parameters (4,25). A fair comparison of the two algorithms is, therefore, only possible if optimization is applied for tuning SVM models.

The overall model performance is decreasing with depth concerning all soil properties as is commonly perceived in pedometric modelling (e.g. 28,52). Figure 7 shows, that this decrease is non-linear. For the topsoil, it usually has very good performance which is then rapidly decreasing at a certain soil depth. The threshold value differs between the soil properties, though. For the particle size distribution (Figures 7A, 7B, and 7C) it lies around 25 cm, for the other soil properties around 10 cm depth (Figures 7D to 7I). Some of the latter have two steps in the performance decrease, one at 10 cm and another at 25 or 30 cm (bulk density, Figure 7E), 30 or 50 cm (symbol_S, Figure 7F), at 40 cm (symbol_G, Figure 7G), or 25 cm (TOC, Figure 7H) depth. The good topsoil performance with regards to the hydromorphic features is probably due to their onset at a certain soil depth. The other step is likely caused by grassland soils not being separated from cropland soils in the SPU differentiation. This could mean that the difference between grassland soils and cropland soils was minor either with regards to the vertical soil profile differentiation and characteristics or regarding the soil-landscape relation. Concerning the latter, the high number of SCORPAN O predictors from remote sensing data provides a good representation of the land cover and would, therefore, easily allow for this separation between the grassland and cropland soils. With the former, it must be taken into account that the difference between the two only affects a limited number of the considered properties and then only the respective topsoil. However, this aspect could only be addressed while the calculation of the property-wise profile difference would assign a higher weight to the topsoil differences for these soil properties. The decision on assigning different weights along the depth profile is not trivial, though. A few test runs were conducted with an exponential weight decay function and a step-wise approach. And optimizing the weights along the depth profile in addition to the ready-implemented optimization tasks in PAMp and PAMm would add to the complexity of the objective function and prolong the optimization process to differentiate the SPUs.

In the following, the multivariate 3D data product will be compared to other ready available data products. This is done by referring to the predictive median RMSE with regards to the interquartile range of the multivariate parameter distributions along the depth profile. On the one hand the property- and depth-wise uncertainty will be compared to its first version from Ließ et al. (4). On the other hand, the national performance estimates (considering agricultural soils) for other spatially continuous data products covering entire Germany were calculated. Table 5 provides an overview. They were evaluated by extracting the predicted property values at the soil survey sites of the test set profile data which had been used to evaluate the here developed data product. The weighted mean was calculated for the respective depth layer before calculating the RMSE. The compared data products have the following spatial raster resolutions: national scale – 100 m (25,55), European scale – 500 m (56) and 1000 m (57), and global scale – 250 m (54).

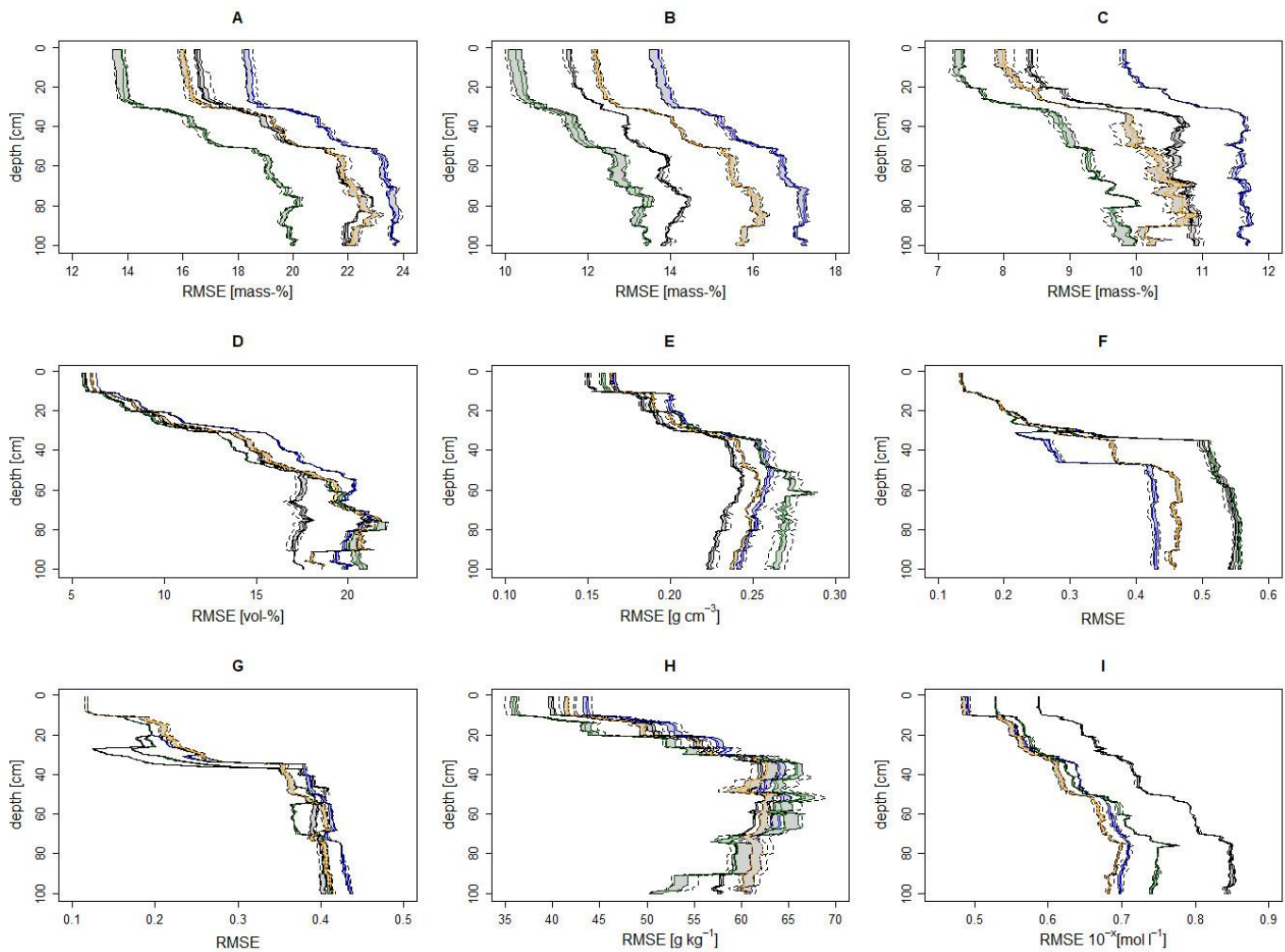


Figure 7: Predictive model performance considering the interquartile range of the SPUS' multivariate distribution along the depth profile. A) sand content, B) silt content, C) clay content, D) stone content, E) bulk density, F) symbol_S, G) symbol_G, H) TOC, and I) pH. The colours reflect the different models: black=RF-PAMP, blue=RF-PAMm, green=SVM-PAMP, yellow=SVM-PAMm. The lines along the shaded area correspond to the lower and upper hinges of the five predicted values' (repeated CV), the solid line to the median, and the dotted lines to the upper and lower whiskers.

With regards to the particle size distribution, the predictive performance improved compared to Ließ et al. (4): For the sand content, it improved from 14.8 to 13.8 mass-% at 20 cm depth, from 17.5 to 16.3 mass-% at 40 cm depth, and from 20.2 to 19 mass-% at 60 cm depth. Respectively, it improved from 10.7 to 10.4, from 12.2 to 11.6, and from 14.3 to 12.7 mass-% for the silt content, and from 8.2 to 7.5, from 10.1 to 8.9, and from 10.1 to 9.3 mass-% for the clay content. Figures 7A, 7B, and 7C show the continuous performance estimates. Concerning the topsoil, the national scale 0-30 cm (25), the European scale 0-20 cm (56), and the global scale 15-30 cm predictions (54) have a higher uncertainty with an RMSE of 15.0, 17.6, and 19.9 mass-% for sand, 11.8, 13.8, and 17.6 mass-% for silt, and 8.2, 9.8, and 11.7 mass-% for clay (Table 5). For the subsoil, the global scale 30-60 cm predictions (54) also have a higher RMSE. It amounts to 22.9 mass-% for sand, 18.7 mass-% for silt, and 13.8 mass-% for clay (Table 5).

Compared to Ließ et al. (4), the predictive performance concerning the stone content remained more or less the same in 20 cm depth with 8.1 versus 8.0 vol-%, improved for 40 cm depth from 14.8 to 13.9 vol-%, but impaired in 60 cm depth from 16.9 to 19.1 vol-%. For the topsoil, the European (0-20 cm) and global scale (15-30 cm) predictions have a slightly higher uncertainty with an RMSE of 9 and 10.5 vol-% (Table 5). Considering the same depth intervals, the

RMSE of the here created data product correspond to an average RMSE of 6.5 vol-% for the 0-20 depth interval, and 9.1 vol-% for the 15-30 cm depth interval. This even higher difference in reference to the European data product is due to the overall decrease in uncertainty with lower soil depth (Figure 7D).

Table 5: National-scale evaluation (RMSE) for existing national, European and global scale data products (considering agricultural soils). The predictive uncertainty was evaluated on behalf of the test set profile data. The values of the raster data products were extracted at the profile sites. A weighted average was calculated for the respective depth interval of the measured data.

Scale of the data product	Depth interval [cm]	Sand content [mass-%]	Silt content [mass-%]	Clay content [mass-%]	Stone content [vol-%]	Bulk density [g cm ⁻³]	TOC [g kg ⁻¹]	pH 10 ^{-x} mol l ⁻¹
National	0-30	15.0 ⁽²⁵⁾	11.8 ⁽²⁵⁾	8.2 ⁽²⁵⁾	-	-	22 ⁽⁵⁵⁾	-
European	0-20	17.6 ⁽⁵⁶⁾	13.8 ⁽⁵⁶⁾	9.8 ⁽⁵⁶⁾	9 ⁽⁵⁶⁾	0.26 ⁽⁵⁶⁾	48.3 ^(57,72)	-
Global ⁽⁵⁴⁾	0-5	19.3	16.5	11.4	7.1	0.30	43.6	1.2
	5-15	19.4	16.4	11.0	7.8	0.30	46.2	1.2
	15-30	19.9	17.6	11.7	10.5	0.31	57.6	1.2
	30-60	22.9	18.7	13.8	17.5	0.35	62.4	1.3
	60-100	25.9	19.6	14.3	21.2	0.36	60.7	1.4

For bulk density, the predictive performance impaired at 20 and 60 cm depth from 0.15 to 0.19, and 0.25 to 0.27 g cm⁻³, but remained the same at 40 cm depth compared to Ließ et al. (4). The predictive topsoil uncertainty is still higher for the European and global data products with an RMSE of 0.26 and 0.31 g cm⁻³, respectively. The same applies to the subsoil with an RMSE of 0.35 g cm⁻³ (global predictions 30-60 cm, Table 5).

The predictive model performance along the depth profile with regards to the TOC is displayed in Figure 7H. TOC was not part of the data product generated by Ließ et al. (4). The averaged RMSE for the respective depth interval is 39.3 compared to 48.3 g kg⁻¹ for Aksoy et al. (57) in the 0-20 cm interval, 43.8 compared to 21 g kg⁻¹ for Sakhaee et al. (55) in the 0-30 cm interval, 38.8 compared to 46.2 g kg⁻¹ in the 5-15 cm, and 49.8 compared to 57.6 g kg⁻¹ in the 15-30 cm interval for Poggio et al. (54). This means the here developed data product has a lower predictive topsoil uncertainty compared to the global and European data products, but a higher uncertainty compared to the national data product. One of the reasons for the latter is the high diversity in the soils containing an organic horizon in some part of their profile. The low number of soil profiles representing these soils in the dataset of the agricultural soil inventory had also caused trouble to Sakhaee et al. (55). They have addressed this aspect by training separate models for organic and mineral topsoil, which resulted in an RMSE decrease from 31.6 to 21.0 g kg⁻¹. The complexity increases, though, while multiple properties are jointly considered in 3D. The optimization to differentiate the SPUs merged all these soils into a single SPU (SPU1, Figure 6 A1). Compared to the high difference in TOC content, between these soils and the all-mineral soils, the TOC differences among the all-mineral soils were minor. Conducting the cluster analysis while applying data transformation to this and other soil properties before calculating the distance matrices did not solve the issue, either. A solution might be to subdivide the data into all-mineral and partly-mineral soils and then conduct two separate optimization processes to differentiate the SPUs in each subgroup as suggested earlier.

The predictive model performance along the depth profile with regards to the pH is displayed in Figure 7I. The pH was not part of the data product generated by Ließ et al. (4). The averaged RMSE for the respective depth interval is 10^{-0.55} compared to 10^{-1.2} mol l⁻¹ in the 5-15 cm, and 10^{-0.58} compared to 10^{-1.2} mol l⁻¹ in the 15-30 cm interval for Poggio et al. (54).

Overall, the here presented models deal with a high complexity: They address the multivariate soil variability in 3D compared to the models trained to obtain the univariate 2D data products. It is impressive that still a lower predictive uncertainty was achieved. The lower uncertainty compared to the European and global data products is likely because at national scale for Germany there are a lot more data proxies available to approximate the soil forming factors, namely the expert information contained in the national map products providing information on the soil distribution (58) and parent material (59,60). This helps in capturing the soil-landscape relation by machine learning. In reference to the national scale data products a higher performance was achieved for texture, but a lower performance for TOC due to the previously mentioned reasons. Finally, it has to be emphasized, that the here presented data product differs from the others. The univariate predictions (single soil property) considered in the comparison provide single-cell predictions for a certain depth interval. In contrast, the here developed data product provides 3D soil information in terms of the multivariate distributions. Its spatial resolution in the 2D mapping space is 100 m, and the resolution along the depth profile is 1 cm. Accordingly, for each raster cell, it provides the slice-wise multivariate distribution of the respective soil properties. It would be inappropriate to consider the median of these distributions for each raster cell. The benefit lies in considering these distributions which are the consequence of condensing the information contained in the raster cells to a limited number of functional SPUs.

3.3.2 Variable importance

The VI values (Figure 8) indicate that all predictors were important to a certain extent for all four models. The values are relative, and not comparable between the models. However, what separates the SVM models (Figures 8C and 8D) from the RF models (Figures 8A and 8B) is the high importance they assign to the categorical predictors in comparison to the other predictors. These categorical predictors reflect the inclusion of expert knowledge with regards to parent material and soils included in conventional map products (BAG00, LIT00, STR00, and BGL00) as well as the classified topography (GMK00). Categorical predictors had also proved highly important for the models of the first implementation to represent the agricultural soil-landscape of Germany by SPUs (4). It is unfortunate in this regard, that further categorical SCORPAN S and SCORPAN P predictors available at a larger map scale could not be included (e.g.17,60). The soil profile database of the agricultural soil inventory does not include sufficient data entries to represent the high number of SMUs included in these maps. The RF models do not prioritize the categorical information, though. This is surprising as they are known to generally favour categorical predictors (62,63). In contrast to the letter, they assign comparatively higher importance to the DEM.

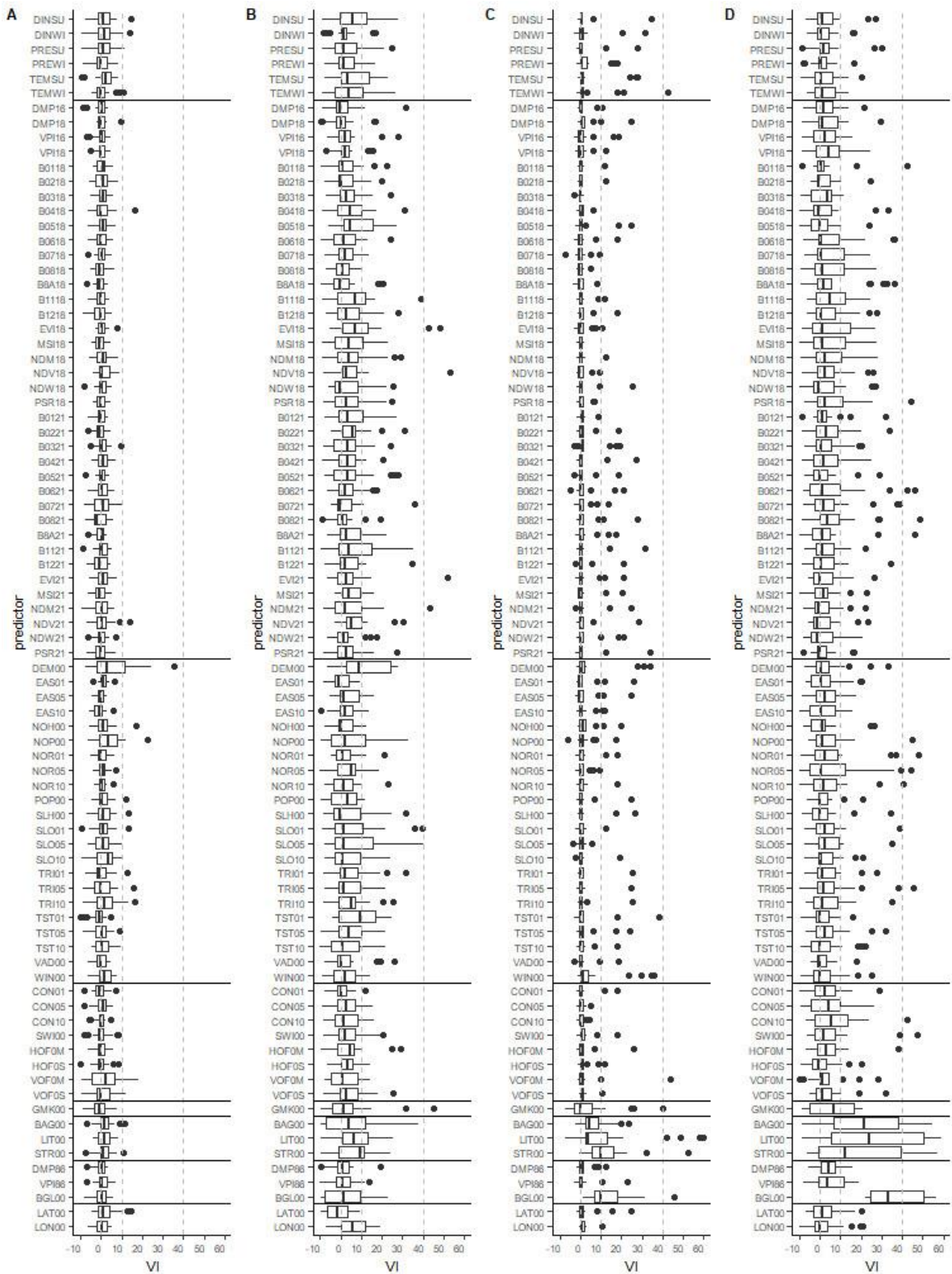


Figure 8: Variable importance (VI) boxplots of the models for SPU regionalization. A) RF-PAMP, B) RF-PAMm, C) SVM-PAMP, and D) SVM-PAMm. The horizontal lines separate the respective predictor groups corresponding to the SCORPAN factors: climate, organisms, relief [topography], relief [hydrology], relief [categorical], parent material, soil, and latitude and longitude. Please refer to Table 1 for the predictor abbreviations.

3.3.3 Nation-wide prediction

Figure 9 displays the map of the nationwide prediction of the SPUs with model SVM-PAMp. In the following, it will be described from north to south according to the four morphologic regions of Germany: The North German Lowland, the Central Germany Uplands, the Alpine Foreland, and the Alps.

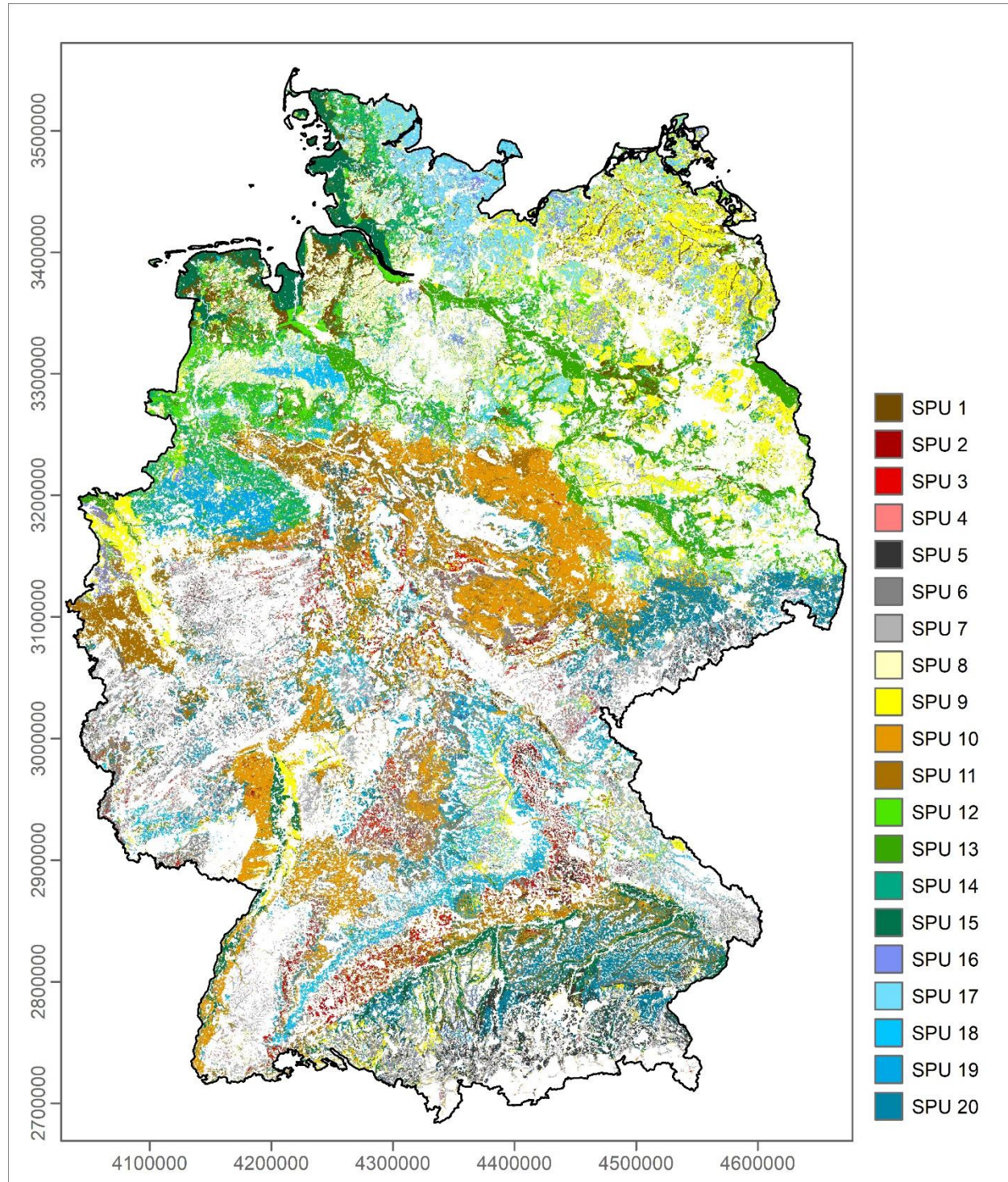


Figure 9: Map of Germany displaying the distribution of the SPUs corresponding to model SVM-PAMp. Colours were selected to emphasize the groups: SPU 1 organic, SPU 2 – SPU 4 leptic–skeletal, SPU 5 – SPU 7 skeletal, SPU 8 – SPU 9 sandy, SPU 10 – SPU 11 silty, SPU 12 – SPU 15 stagnic, and SPU 16 – SPU 20 gleyic SPUs. Non-agricultural areas are masked.

The North German Lowland presents a mixture of sandy soils (SPU8, SPU 9), stagnic soils (SPU 12 – SPU 15) gleyic soils (SPU 16 – SPU 19) and patches of the organic SPU 1. Of the sandy soils, SPU 8 dominates in the west and SPU 9 in the east. SPU 8 has higher sand and correspondingly lower pH values (Figures 6B8, 6B9, 6J8, and 6J9). The higher topsoil TOC values of SPU 8 likely originate from the land-use history in this region. Nutrient-poor, sandy topsoil was often improved by mixing it with grass or heather plagues (4). Stagnic SPU 15 is found along the North Sea coast in the marshland under tidal influence. It is this stagnic SPU which differs from the other stagnic SPUs due to its much lower sand and correspondingly higher silt and clay contents. SPU 14 is dominating in the northern-most part right between the North and Baltic Sea. It is the stagnic SPU whose stagnic properties start at a higher soil depth compared to the others. SPU 12 and SPU 13 are found in the floodplains and lower terraces of the rivers Weser, Elbe, and Oder. The gleyic soils in the north are dominated by SPU 17 along the east coast (Baltic Sea) with patches of this SPU as well as SPU 16, SPU 18, and SPU 19 further inland. SPU 14 and SPU 19 also dominate the area in the south-westernmost part of the North German lowland corresponding to the lowlands of the glacial valleys of the old moraine area (58).

In the Central German Uplands, the Loess plains are represented by SPU 10 and SPU 11. Considering their multivariate distributions, they are mainly differentiated by their pH, with SPU 10 having the higher pH values (Figures 6J10 and 6J11). The gleyic SPU 20 dominates the loess plains in Saxony. It has similarly high silt contents as SPU 10 and SPU 11. However, large parts of the Central German Uplands are covered by the leptic–skeletal SPUs 2 – 4 and skeletal SPUs 5 – 7, which are distinguished by their high stone contents. Of these, SPU 7 with much lower sand contents and correspondingly higher pH values (compared to SPU 5 and SPU 6) is dominating. Still, large parts along the Swabian Alp, the Franconian Alp, Spessart, and Franconian Switzerland are displaying a high coverage by leptic–skeletal SPU 2, the SPU with the highest depth limitation. The gleyic SPU 18 covers large parts along these mountain ranges. The lower Rhine valley stands out by the domination of sandy SPU 9. Between the cities Karlsruhe and Mainz, SPU 9 is then accompanied by the stagnic SPU 15 with its much lower sand contents. SPU 15 also dominates along the floodplains of the Danube and tributary rivers, which separates the Central German Uplands from the Alpine Foreland. Regarding the considered soil properties, these soils are similar to those along the North Sea coast. To distinguish them from one another, additional soil properties would have to be included. The soils might differ in their electrical conductivity due to the tidal influence along the North Sea coast.

Large parts of the North-East of the Alpine Foreland are covered by the silty SPU 10 as well as the gleyic SPU 20, having a similar texture. It indicates the similarity of these soils to the Loess plains. And they are co-occurring with gleyic SPU 16 having higher sand contents. Large parts of the remaining region are dominated by the leptic–skeletal SPU 2 and SPU 4, while patches of the sandy SPU 9 and organic SPU 1 are also clearly distinguishable. Large parts of the Alps are not under agricultural use. Those that are, often contain high stone contents (SPU 3, SPU 5, and SPU 6) and are partly limited in depth (SPU 3). Still, the sandy SPU 9, silty SPU 10, stagnic SPU 15, and gleyic SPU 16 also occur.

Overall the number of SPUs and respective spatially allocated SPUs increased from 8 to 20 in comparison to Ließ et al. (4) providing a more detailed spatial differentiation. The previous single SPU with a high stone content and a depth limitation in the top 100 cm, now augmented to six SPUs with a high stone content of which three additionally have a depth limitation in their top 100 cm. The two SPUs with stagnic and two with gleyic properties augmented to four and five respectively. The SPUs with a predominantly sandy or silty texture augmented from one SPU to two SPUs in both cases. Merely, the SPU including soils with organic horizons remained only one, another hint to consider the separate differentiation into SPUs for the all-mineral and partly-mineral soils.

The pattern of the spatial allocation of the SPUs shows some similarity with regards to the national scale soil map products BÜK200 and BÜK1000 (17,64). This was expected considering the high importance of the SCORPAN P, SCORPAN R, and SCORPAN S predictors. Ultimately, the national soil maps also heavily rely on topography and

parent material. As mentioned previously, the information contained in the spatial units differs. Complex SMUs composed of multiple co-occurring soils differing largely in their profile characteristics are by no means comparable to spatially allocated SPUs each being described by a multivariate parameter distribution along the depth profile. It is interesting to notice, though, that the here provided data product is a national-scale representation with much fewer SPUs as there are SMUs in these soil maps.

4 Conclusions

The national-scale evaluation and modelling of the impact of agricultural management and climate change on soils, crop growth, and the environment require soil information at a spatial resolution addressing individual agricultural fields. The agglomeration of the soil parameter space into a limited number of functional SPUs allows for reducing the required resources to run agricultural process models without having to cut back on the spatial resolution. To serve these needs, creative data science approaches are needed.

Here, two data science approaches were developed involving unsupervised classification to generate a multivariate 3D data product of spatially allocated functional SPUs each being defined by a multivariate parameter distribution along the depth profile from 0 to 100 cm. The two methods account for differences in variable types and distributions and involve genetic algorithm optimization to identify those SPUs with the lowest internal variability and maximum inter-unit difference with regards to both, their soil characteristics and landscape setting.

The high potential of these two approaches was demonstrated by applying them to the agricultural German soil landscape. The resulting data product consists of twenty SPUs which are each described by a multivariate parameter distribution along the depth profile from 0 to 100 cm. It comes along with property- and depth-wise uncertainty estimates. Its spatial resolution in the 2D mapping space is 100 m, and the resolution along the depth profile is 1 cm. It is available in a reduced storage format consisting of two related files, [1] a nationwide raster file with identifiers pointing to [2] the respective multivariate distribution for each functional SPU provided in table format. Each property's distribution is represented by the 5, 25, 50, 75 and 95% quantiles.

The spatial pattern of the nationwide raster shows some similarity with the national soil maps of Germany. The information contained in the spatial units differs, though. Complex SMUs composed of multiple co-occurring SUs of very different characteristics are by no means comparable to the spatially allocated SPUs that are each represented by a multivariate parameter distribution. Furthermore, it is interesting that the here created data product is a national-scale representation with much fewer SPUs as there are SMUs in these soil maps. And the boundaries of the SPUs differ from those of the SMUs. Why the boundaries differ and whether the number of SPUs would increase while a larger soil profile database would be included, are two aspects which are valuable to investigate together with colleagues from the soil survey institutes.

The created data product is the second version of such a 3D soil-landscape model for the agricultural landscape of Germany. Compared to Version 1, the number of SPUs increased, and the respective interquartile range of the multivariate distributions and the predictive uncertainty were reduced. Additionally, two further soil properties, TOC and pH, were included. Version 2 of the data product also has a lower uncertainty compared to existing univariate 2D data products while considering the interquartile range of the multivariate distributions. I recommend using them as margins to run agricultural process models. Limitations concerning TOC uncertainty suggest considering all-mineral and partly-mineral soils separately in the SPU differentiation. Whether the available data is sufficient to follow such an approach would have to be tested, though.

Data Availability Statement

The data product for this study will be published open access upon acceptance of the manuscript.

Funding

This work was funded by the German Federal Ministry of Education and Research (BMBF) in the framework of the funding measure Soil as a Sustainable Resource for the Bioeconomy – BonaRes, project BonaRes (Module B): BonaRes Centre for Soil Research (grant 031B0511). For further information please visit www.bonares.de.

References

1. Kapoor D, Bhardwaj S, Landi M, Sharma A, Ramakrishnan M, Sharma A. The impact of drought in plant metabolism: How to exploit tolerance mechanisms to increase crop production. *Appl Sci* (2020) 10: doi: 10.3390/app10165692
2. Magombeyi MS, Taigbenu AE, Barron J. Effectiveness of agricultural water management technologies on rainfed cereals crop yield and runoff in semi-arid catchment: a meta-analysis. *Int J Agric Sustain* (2018) 16:418–441. doi: 10.1080/14735903.2018.1523828
3. Hatfield JL, Dold C. Water-use efficiency: Advances and challenges in a changing climate. *Front Plant Sci* (2019) 10:1–14. doi: 10.3389/fpls.2019.00103
4. Ließ M, Gebauer A, Don A. Machine Learning With GA Optimization to Model the Agricultural Soil-Landscape of Germany: An Approach Involving Soil Functional Types With Their Multivariate Parameter Distributions Along the Depth Profile. *Front Environ Sci* (2021) 9:1–24. doi: 10.3389/fenvs.2021.692959
5. Searle R, McBratney A, Grundy M, Kidd D, Malone B, Arrouays D, Stockman U, Zund P, Wilson P, Wilford J, et al. Digital soil mapping and assessment for Australia and beyond: A propitious future. *Geoderma Reg* (2021) 24: doi: 10.1016/j.geodrs.2021.e00359
6. Mueller L, Schindler U, Mirschel W, Graham Shepherd T, Ball BC, Helming K, Rogasik J, Eulenstein F, Wiggering H. Assessing the productivity function of soils. A review. *Agron Sustain Dev* (2010) 30:601–614. doi: 10.1051/agro/2009057
7. Tolosan C, Sciences P, Tech GA, Conservation R, Evaluation L, Centre D, Canada A, Republic C, Centre D, Canada A, et al. Calibration of crop phenology models : Going beyond A major effect of environment on crops is through crop phenology , and therefore , the capacity to Key words crop model , prediction error , protocol , model ensemble , variability. (2022). 1–26 p.
8. Boeing F, Rakovech O, Kumar R, Samaniego L, Schrön M, Hildebrandt A, Rebmann C, Thober S, Müller S, Zacharias S, et al. High-resolution drought simulations and comparison to soil moisture observations in Germany. *Hydrol Earth Syst Sci Discuss* (2021) 1–35.
9. Bönecke E, Breitsameter L, Brüggemann N, Chen TW, Feike T, Kage H, Kersebaum KC, Piepho HP, Stützel H. Decoupling of impact factors reveals the response of German winter wheat yields to climatic changes. *Glob Chang Biol* (2020) 26:3601–3626. doi: 10.1111/gcb.15073
10. Webber H, Lischeid G, Sommer M, Finger R, Nendel C, Gaiser T, Ewert F. No perfect storm for crop yield failure in Germany.

Environ Res Lett (2020) 15: doi: 10.1088/1748-9326/aba2a4

11. Drastig K, Prochnow A, Libra J, Koch H, Rolinski S. Irrigation water demand of selected agricultural crops in Germany between 1902 and 2010. *Sci Total Environ* (2016) 569–570:1299–1314. doi: 10.1016/j.scitotenv.2016.06.206
12. Chen S, Arrouays D, C. DAA, Chenu C, Barré P, Martin MP, Saby NPA, Walter C. National estimation of soil organic carbon storage potential for arable soils: a data-driven approach coupled with carbon-landscape zones. *Sci Total Environ* (2019)
13. Wiesmeier M, Urbanski L, Hobley E, Lang B, von Lützow M, Marin-Spiotta E, van Wesemael B, Rabot E, Ließ M, Garcia-Franco N, et al. Soil organic carbon storage as a key function of soils - A review of drivers and indicators at various scales. *Geoderma* (2019) 333: doi: 10.1016/j.geoderma.2018.07.026
14. Wang C, Amon B, Schulz K, Mehdi B. Factors that influence nitrous oxide emissions from agricultural soils as well as their representation in simulation models: A review. *Agronomy* (2021) 11: doi: 10.3390/agronomy11040770
15. Bouraoui F, Grizzetti B. Modelling mitigation options to reduce diffuse nitrogen water pollution from agriculture. *Sci Total Environ* (2014) 468–469:1267–1277. doi: 10.1016/j.scitotenv.2013.07.066
16. Sundermann G, Wäagner N, Cullmann A, von Hirschhausen CR, Kemfert C. *Nitrate pollution of groundwater long exceeding trigger value: Fertilization practices require more transparency and oversight*. DIW Weekly. Berlin: Deutsches Institut für Wirtschaftsforschung (DIW) (2020). Vol. 10, Iss. 8/9, pp. 61–72 p. doi: http://dx.doi.org/10.18723/diw_dwr:2020-8-1
17. BGR. *Soil Map of Germany 1:250,000*. Hanover: Federal Institute for Geosciences and Natural Resources (2018).
18. Ad-hoc-AG Boden. *Bodenkundliche Kartieranleitung. KA5*. 5th ed. Stuttgart, Germany: Bundesanstalt für Geowissenschaften und Rohstoffe in Zusammenarbeit mit den Staatlichen Geologischen Diensten (2005). http://www.schweizerbart.de/publications/detail/isbn/9783510959204/Bodenkundliche_Kartieranleitung_5_Aufl
19. Jenny H. *Factors of Soil Formation. A System of Quantitative Pedology*. New York: Dover Publications, Inc. (1941).
20. McBratney AB, Mendonca Santos ML, Minasny B. *On digital soil mapping*. (2003). 3–52 p. doi: 10.1016/S0016-7061(03)00223-4
21. Padarian J, Minasny B, Mcbratney AB. Machine learning and soil sciences : A review aided by machine learning tools. *SOIL* (2019) discussion: <https://doi.org/10.5194/soil-2019-57>
22. Arrouays D, Mulder VL, Richer-de-Forges AC. Soil mapping, digital soil mapping and soil monitoring over large areas and the dimensions of soil security – A review. *Soil Secur* (2021) 5:100018. doi: 10.1016/j.soisec.2021.100018
23. Chen S, Arrouays D, Leatitia Mulder V, Poggio L, Minasny B, Roudier P, Libohova Z, Lagacherie P, Shi Z, Hannam J, et al. Digital mapping of GlobalSoilMap soil properties at a broad scale: A review. *Geoderma* (2022) 409:115567. doi: 10.1016/j.geoderma.2021.115567
24. Žížala D, Minařík R, Beitlerová H, Juřicová A, Skála J, Rojas JR, Penížeck V, Zádorová T. High-Resolution Soil Property Maps from Digital Soil Mapping Methods, Czech Republic. *SSRN Electron J* (2021)1–53. doi: 10.2139/ssrn.3928321
25. Gebauer A, Sakhaee A, Don A, Poggio M, Ließ M. Topsoil Texture Regionalization for Agricultural Soils in Germany—An Iterative Approach to Advance Model Interpretation. *Front Soil Sci* (2022) 1:1–21. doi: 10.3389/fsoil.2021.770326

26. Malone B, Searle R. Updating the Australian digital soil texture mapping (Part 2): spatial modelling of merged field and lab measurements. *Soil Res* (2021) 59:419–434. doi: 10.1071/SR20283
27. Reddy NN, Chakraborty P, Roy S, Singh K, Minasny B, McBratney AB, Biswas A, Das BS. Legacy data-based national-scale digital mapping of key soil properties in India. *Geoderma* (2021) 381:114684. doi: <https://doi.org/10.1016/j.geoderma.2020.114684>
28. Padarian J, Minasny B, McBratney AB. Using deep learning for digital soil mapping. *Soil* (2019) 5:79–89. doi: 10.5194/soil-5-79-2019
29. Ma Y, Minasny B, McBratney A, Poggio L, Fajardo M. Predicting soil properties in 3D: Should depth be a covariate? *Geoderma* (2021) 383: doi: 10.1016/j.geoderma.2020.114794
30. Poeplau C, Don A, Flessa H, Heidkamp A, Jacobs A, Prietz R. First German Agricultural Soil Inventory – Core dataset. (2020) doi: 10.3220/DATA20200203151139
31. Jacobs A, Flessa H, Don A, Heidkamp A, Prietz R, Dechow R, Gensior A, Poeplau C, Riggers C, Schneider F, et al. Landwirtschaftlich genutzte Böden in Deutschland - Ergebnisse der Bodenzustandserhebung. (2018). 321 p. doi: 10.3220/REP1542818391000
32. INSPIRE TWG. *INSPIRE - Infrastructure for Spatial Information in Europe. D2.8.I.2 Data Specification on Geographical Grid Systems– Technical Guidelines*. INSPIRE Thematic Working Group Coordinate Reference Systems & Geographical Grid Systems, European Commission (2014).
33. Conrad O, Bechtel B, Bock M, Dietrich H, Fischer E, Gerlitz L, Wehberg J, Wichmann V, Böhner J. System for Automated Geoscientific Analyses (SAGA) v. 2.1.4. *Geosci Model Dev* (2015) 8:1991–2007. doi: 10.5194/gmd-8-1991-2015
34. Kaufman L, Rousseeuw PJ. *Finding Groups in Data: An Introduction to Cluster Analysis*. New York: John Wiley & Sons (1990).
35. Ahmad A, Khan SS. Survey of State-of-the-Art Mixed Data Clustering Algorithms. *IEEE Access* (2019) 7:31883–31902. doi: 10.1109/ACCESS.2019.2903568
36. Van Mechelen I, Boulesteix A-L, Dangi R, Dean N, Guyon I, Hennig C, Leisch F, Steinley D. Benchmarking in cluster analysis: A white paper. (2018)1–23. <http://arxiv.org/abs/1809.10496>
37. Breiman L. Random Forests. *J Chem Inf Model* (2001) 53:1689–1699. doi: 10.1017/CBO9781107415324.004
38. Breiman L. Random forest. *Mach Learn* (2001) 45:5–32.
39. Hothorn T, Hornik K, Strobl C, Zeileis A. Package “party”. A Laboratory for Recursive Partytioning. Version 1.1-2. (2016).
40. Ishwaran H, Kogalur UB. Package ‘randomForestSRC’. Random Forests for Survival, Regression and Classification. (2016)
41. Cortes C, Vapnik V. Support-Vector Networks. *Mach Learning* (1995) 20:273–297. doi: <http://dx.doi.org/10.1007/BF00994018>
42. Chang C-C, Lin C-J. LIBSVM: A Library for support vector machines. *ACM Trans Intell Syst Technol* (2011) 2:1–39. doi: 10.1145/1961189.1961199

43. Meyer D. Support Vector Machines - The Interface to libsvm in package e1071. *FH Tech Wien* (2019) 16:130. <http://www.csie.ntu.edu.tw/~cjlin/papers/ijcnn.ps.gz>
44. Hastie T, Tibshirani R, Friedman J. *The Elements of Statistical Learning*. (2009). 1–694 p. doi: 10.1007/b94608
45. Affenzeller M, Winkler S, Wagner S, Beham A. *Genetic algorithms and genetic programming*. Boca Raton: Taylor and Francis Group (2009).
46. Batjes N. A taxotransfer rule based approach for filling gaps in measured soil data in primary SOTER databases. *ISRIC-World Soil Information, Wageningen* (2003) http://www.isric.org/isric/webdocs/docs/ISRIC_Report_2003_03.pdf
47. Hugelius G, Bockheim JG, Camill P, Elberling B, Grosse G, Harden JW, Johnson K, Jorgenson T, Koven CD, Kuhry P, et al. A new data set for estimating organic carbon storage to 3 m depth in soils of the northern circumpolar permafrost region. *Earth Syst Sci Data* (2013) 5:393–402. doi: 10.5194/essd-5-393-2013
48. Almendra-Martín L, Martínez-Fernández J, Piles M, González-Zamora Á. Comparison of gap-filling techniques applied to the CCI soil moisture database in Southern Europe. *Remote Sens Environ* (2021) 258:112377. doi: 10.1016/j.rse.2021.112377
49. Wang Q, Wang L, Zhu X, Ge Y, Tong X, Atkinson PM. Remote sensing image gap filling based on spatial-spectral random forests. *Sci Remote Sens* (2022) 5:100048. doi: 10.1016/j.srs.2022.100048
50. Taki R, Wagner-Riddle C, Parkin G, Gordon R, VanderZaag A. Comparison of two gap-filling techniques for nitrous oxide fluxes from agricultural soil. *Can J Soil Sci* (2019) 99:12–24. doi: 10.1139/cjss-2018-0041
51. Kim Y, Johnson MS, Knox SH, Black TA, Dalmagro HJ, Kang M, Kim J, Baldocchi D. Gap-filling approaches for eddy covariance methane fluxes: A comparison of three machine learning algorithms and a traditional method with principal component analysis. *Glob Chang Biol* (2020) 26:1499–1518. doi: 10.1111/gcb.14845
52. Ghanbarian B, Pachepsky Y. Machine learning in vadose zone hydrology: A flashback. *Vadose Zo J* (2022)doi.org/10.1002/vzj2.20212. doi: 10.1002/vzj2.20212
53. Lamichhane S, Kumar L, Wilson B. Digital soil mapping algorithms and covariates for soil organic carbon mapping and their implications: A review. *Geoderma* (2019) 352:395–413. doi: <https://doi.org/10.1016/j.geoderma.2019.05.031>
54. Poggio L, De Sousa LM, Batjes NH, Heuvelink GBM, Kempen B, Ribeiro E, Rossiter D. SoilGrids 2.0: Producing soil information for the globe with quantified spatial uncertainty. *Soil* (2021) 7:217–240. doi: 10.5194/soil-7-217-2021
55. Sakhaee A, Gebauer A, Ließ M, Don A. Performance of three machine learning algorithms for predicting soil organic carbon in German agricultural soil. (2021)1–24.
56. Ballabio C, Panagos P, Monatanarella L. Mapping topsoil physical properties at European scale using the LUCAS database. *Geoderma* (2016) 261:110–123. doi: 10.1016/j.geoderma.2015.07.006
57. Aksoy E, Yigini Y, Montanarella L. Combining soil databases for topsoil organic carbon mapping in Europe. *PLoS One* (2016) 11:2022. doi: 10.1371/journal.pone.0152098
58. BGR. *Soil Scapes in Germany 1:5,000,000. BGL5000. Hanover:*. Hanover: Federal Institute for Geosciences and Natural

Resources (2008).

59. BGR. *Groups of soil parent material in Germany 1:5,000,000. BAG5000, Version 3.0.* Hanover: Federal Institute for Geosciences and Natural Resources (2008).
60. BGR and SDG. *Hydrogeological Map of Germany 1:250,000 (HÜK250).* Hanover: Federal Institute for Geosciences and Natural Resources (BGR) and German State Geological Surveys (SGD) (2019).
61. BGR. *General Geological Map of the Federal Republic of Germany 1:200,000.* Hanover: Federal Institute for Geosciences and Natural Resources (2007).
62. Probst P, Wright MN, Boulesteix AL. Hyperparameters and tuning strategies for random forest. *Wiley Interdiscip Rev Data Min Knowl Discov* (2019) 9:1–15. doi: 10.1002/widm.1301
63. Strobl C, Boulesteix A-L, Zeileis A, Hothorn T. Bias in random forest variable importance measures: illustrations, sources and a solution. *BMC Bioinformatics* (2007) 8:25. doi: 10.1186/1471-2105-8-25
64. BGR. *Soil Map of Germany 1:1,000,000. BÜK1000.* Hanover: Federal Institute for Geosciences and Natural Resources (2013).
65. DWD. Seasonal grids of sum of precipitation over Germany, version v1.0. (2018)
66. DWD. Seasonal grids of monthly averaged daily air temperature (2m) over Germany, version v1.0. (2018)
67. DWD. Seasonal grids of sum of drought index (de Martonne) over Germany, version v1.0. (2018)
68. Swinnen E, Van Hoolst R. Copernicus Global Land Operations "Vegetation and Energy". Issue I1.12, Version 1. (2019) https://land.copernicus.eu/global/sites/cgls.vito.be/files/products/CGLOPS1_ATBD_DMP300m-V1_I1.12.pdf
69. Swinnen E, Toté C. Gio Global Land Component - Lot I "Operation of the Global Land Component", Algorithm Theoretical Basis Document, Issue I2.11. *Algorithm Theor Basis Doc Issue I211* (2015)1–31. http://land.copernicus.eu/global/sites/default/files/products/GIOGL1_ATBD_SAV1_I1.01.pdf
70. BGR. *Geomorphographic Map of Germany, GMK1000.* Hanover: Federal Institute for Geosciences and Natural Resources (2007).
71. European Environment Agency (EEA). Copernicus Land Monitoring Service - EU-DEM. European Digital Elevation Model Version 1.1. (2017) <https://www.eea.europa.eu/data-and-maps/data/copernicus-land-monitoring-service-eu-dem>
72. Van Liedekerke M, Panagos P. Predicted distribution of SOC content in Europe (based on LUCAS, BioSoil and CZO) in the context of the EU-funded SoilTrEC project. (2016). esdac.jrc.ec.europa.eu